https://doi.org/10.1016/j.jclepro.2020.120225

Techno-economic evaluation and technology roadmap of the MWe-scale SOFC-PEMFC hybrid fuel cell system for clean power generation

Hongli Yan[a], Guoping Wang[a], Zuowei Lu[a], Peng Tan[b,c], Trevor Hochsun Kwan[c], Haoran Xu[b], Bin Chen[b], Meng Ni[b,*], Zhen Wu[b,d,*]

[a]*Department of Mechanical Engineering, Xi'an Jiaotong University City College, Xi'an, China*

[b]*Building Energy Research Group, Department of Building and Real Estate, The Hong Kong Polytechnic University, Hong Kong, China*

[c]*Department of Thermal Science and Energy Engineering, University of Science and Technology of China, Hefei 230026, Anhui, China*

[d]*Shaanxi Key Laboratory of Energy Chemical Process Intensification, School of Chemical Engineering and Technology, Xi'an Jiaotong University, Xi'an, China*

*Corresponding author, Email: meng.ni@polyu.edu.hk (M Ni) wuz2015@mail.xjtu.edu.cn (Z Wu)

ABSTRACT: This paper proposes a novel hybrid fuel cell power generation system with high efficiency. The thermo-economic modeling of the MWe-scale systems using different fuels is conducted to evaluate the economic feasibility under the subsidy policy of Eastern China. This work aims to develop the technology roadmap for this kind of clean power system. It is found that natural gas and biogas fed systems could reach up to 64% and 63.5% respectively, thus they are efficient and cost-optimal for the hybrid system while liquefied petroleum gas and water gas yield low efficiency and high electricity cost. Moreover, under the subsidy policy, the biogas-fed hybrid system is more suitable for a small-scale power system, while the natural gas-fed system is preferable for the large-scale case. The specific electricity cost of small-scale biogas hybrid fuel cell power plant is 0.365 CNY/kWh, lower than the present feed-in-tariff price 0.475~0.704 CNY/kWh of other biogas plants in China. Also, the cost of 0.345~0.347 CNY/kWh of large-scale natural gas-fed hybrid system is much lower than the on-grid electricity price 0.7655 CNY/kWh in Shanghai. These results reveal that the proposed hybrid fuel cell power system is efficient and economically feasible. The payback period and annual return on investment are 0.8~1.2 year and 11~12%, respectively.

Keywords: Fuel cell; Hybrid system; Techno-economic performance; Power generation; Alternative fuels

Nomenclature

Symbols

A	area, m^2
C	cost, CNY
C_d	hydrogen desorption reaction rate constant, s^{-1}
Cp	specific heat capacity, J kg^{-1} K^{-1}
D^{eff}	effective diffusion coefficient, m s^{-1}
E_{act}	activation energy, J mol^{-1}
E_N	reversible voltage, V
F	Faraday constant, C mol^{-1}
$\frac{H}{M}$	hydrogen and metal atomic ratio
I	current, A
J	current density, A m^{-2}
J_0	exchange current density, A m^{-2}
K	reaction equilibrium constant
k	frequency factor of catalyst, kmol kg^{-1} s^{-1} bar^{-1}
LHV_{fuel}	lower heating value of fuel, kW
L_{Pt}	amount of catalyst Pt load, mg cm^{-2}
l	thickness, mm
n_{cycle}	number of cycles
P	power, kW
p	pressure, bar
R_g	universal gas constant, J K^{-1} mol^{-1}

$SEEC$	specific electric energy cost, CNY/kW h
T	temperature, K
t	time, h
U	volume, m^3
V	voltage, V
W	energy consumption, kW
X	reaction fraction
ϕ	mass flow, kg s^{-1}
$\triangle H$	reaction enthalpy, J mol^{-1}
η	energy efficiency
ρ	density, kg m^{-3}
λ	cycle life time, year
$\dot{m}$	H_2 flow velocity, mol s^{-1}
ω_{MH}	MH price, CNY kg^{-1}
ψ_{MH}	hydrogen capacity, wt%
π_{NG}	NG price, CNY m^{-3}
θ	FC degradation factor
γ	scale exponent

Subscript

a	anode
act	activation
AUX	auxiliary
c	cathode
$capt$	capital
$cata$	catalyst
$comp$	compressor
$conc$	concentration

cool	coolant
DC/AC	direct/alternating current
Depr	depreciation
e	electrolyte
eq	equilibrium
g	gas
Gross	gross
h	high-temperature
HE	heat exchanger
hot	hot fluid
HSA	hydrogen storage alloy
in	inlet
ISE	isentropic
Ins	insurance
Int	interest
INV	inverter
l	low-temperature
max	maximum
Main	maintenance
MEC	mechanical
MH	metal hydride
MSR	methane steam reforming
Net	net
ohm	ohmic
oper	operation
PEM	proton exchange membrane
reac	reactor
ref	reference

SOFC	solid oxide fuel cell
TSA	thermal swing adsorption
WGS-cata	catalyst of water gas shift reaction
WGS-reac	water gas shift reactor

1. Introduction

With the rapid recent development of the human society and economy, the energy consumption has been dramatically increasing (The World Bank, 2018; Wang et al., 2019). The consumption of traditional fossil fuels such as oil and coal has resulted in serious environmental pollution issues. Besides, the quantity of fossil fuels is significantly decreasing and its energy conversion efficiency by conventional thermal power plant is generally low (Feron et al., 2019; Fiorentino et al., 2019). Therefore, it is urgent to develop clean and efficient energy conversion technologies using fossil or alternative fuels to meet the rapidly growing demand for energy. The clean fuels such as natural gas (NG) and biogas, are attracting more and more attention because of their high energy conversion efficiency, abundant resources, environmental-friendliness and economic benefits (Calbry-Muzyka et al., 2019; Meng et al., 2019). For example, Mehrpooya et al. reported a novel cascading power cycle or supercritical CO_2 power cycle based on the liquefied natural gas (LNG) unit for power generation (Mehrpooya et al., 2018a, 2018b). Additionally, the biogas resource can be derived from forest residues, domestic and industrial organic wastes, livestock manure, and crop residues. Since NG and biogas are the third and fourth largest energy sources in the world (Congress US, 2005; International Energy Agency, 2018), many countries have paid their attention to the development of the NG and biogas utilization technology all around the world. In such a context, the high-efficiency and clean utilization technology of these low carbon fuels is greatly advocated in an urgent manner to alleviate the energy crisis and environmental pollution.

It is well known that fuel cell (FC) power technology is an innovative and promising power generation technology due to high energy conversion efficiency, low environmental impact and low noise (Damo et al., 2019). The commonly used FCs are solid oxide fuel cell

(SOFC), proton exchange membrane fuel cell (PEMFC), phosphoric acid fuel cell (PAFC), alkaline fuel cell (AFC), and molten carbonate fuel cell (MCFC). Among the FCs, the SOFC is required to work at high operating temperatures of more than 600 ℃ (Tang et al., 2016), which enables the use of various hydrocarbon fuels as the fuel for power generation. Owing to the high operation temperatures, internal resistive losses and the large exothermic heat (242 kJ/mol) of the electrochemical reaction, a significant portion of the consumed fuel is converted into waste heat which is normally carried into the SOFC flue gases. Therefore, the single high-temperature FC has a relatively low net electricity efficiency. To improve the electric yield, an effective approach is to develop the hybrid energy system for power generation such as including a gas turbine (GT) to yield additional power from the generated waste heat. Alternatively, Mehrpooya et al. developed a novel hybrid fuel cell system coupling CO_2 capturing process based on MCFC (Mehrpooya et al., 2017a). It was found that the net electricity efficiency of the hybrid system reaches up to 60.1%. Gholamian et al proposed a hybrid system that consists of a PEMFC, thermoelectric generator and organic Rankine cycle (ORC) for power and hydrogen production (Gholamian et al., 2018). It was found that the heat recovery by thermoelectric generator helps to increase the exergy efficiency by 21.9% compared with the basic ORC system for power generation.

The SOFC is highly adaptable and robust to fuel flexibility (such as NG, biogas, petroleum gas and so on). Meanwhile, the high operating temperature enables the SOFC exhaust gas with a large amount of waste heat to drive bottomed thermodynamic cycles. Therefore, more and more attention has been paid on the integration of SOFC to energy conversion systems and ultimately improving the energy conversion efficiency (Lv et al., 2019). Habibollahzade et al. investigated the biomass-fed SOFC-Stirling engine-electrolyzer hybrid power system based on multi-objective optimization method (Habidollahzade et al., 2018). This kind of hybrid system presents the increased power generation/exergy efficiency and reduced cost compared with the SOFC-gasifier combined system. The improved performance is mainly ascribed to the high degree of waste heat recovery (Mehrpooya et al., 2017b). Actually, the SOFC-GT hybrid power system has been primarily investigated in recent years (Rossi et al., 2019; Habibollahzade et al., 2019). It has been successfully proven that the combination of SOFC and GT facilitates the

improvement of electrical efficiency and the reduction of capital costs. Sghaier et al. concluded that the integration of SOFC and GT could significantly enhance the overall cycle efficiency (more than 60%) through an energetic and exergetic parametric study (Sghaier et al., 2018). Liu et al. designed a novel CCHP (combined cooling, heating and power) system to achieve cascade energy utilization and CO_2 capture, which consists of SOFC, GT, CO_2 cycle, ORC, and LNG cold cycle (Liu et al., 2019). The proposed CCHP system exhibits a high energy utilization efficiency with near zero emissions, whose overall exergy efficiency can reach up to 62.29%.

In addition to power generation, with small modifications to the stack structure, the SOFC can also act like a reformer to produce H_2 as well. Such H_2 can then be delivered to the PEMFC for additional power generation. Since the FC has the higher net electricity efficiency than the GT, the SOFC-PEMFC hybrid system is more suitable as a distributed energy source based power plant than the SOFC-GT hybrid system. Also, this hybrid fuel cell system for power generation is much cleaner. Therefore, the SOFC-PEMFC hybrid power system has been attracting more and more attention. Vollmar et al. first introduced the innovative concept of the SOFC-PEMFC hybrid system, and from a thermal point of view, the heating values of the H_2 and syngas produced from the SOFC are higher grade than the generated waste heat from the electrochemical reactions (Vollmar et al., 2008). It was reported that the energy conversion efficiency of the SOFC-PEMFC hybrid system is improved by 8%~16% compared with standalone SOFC system (Rabbani and Rokni, 2014). However, impurity gases (CO, CO_2), which appear as by-products of the electrochemical reactions, will usually be carried into the SOFC exhaust gas. These impurity gases have a negative impact on the PEMFC performance in terms of material degradation and blockage of the reactants. Generally, pure H_2 of over 99.97% is preferred as the input. Thus, a gas processing (GP) unit should be coupled between SOFC and PEMFC for H_2 separation and purification to ensure high-purity H_2 as the fuel for PEMFC. To achieve this, Fernandes et al. employed a pressure swing adsorption (PSA) for H_2 separation to connect the reforming output and the PEMFC anode input in the hybrid system (Fernandes et al., 2016). Although the PSA method is simple operation and low cost, the produced H_2 purity is not high enough to meet the demand of PEMFC for H_2 purity. The H_2

purity by four-bed PSA was reported to be 96-99.5% (Ahn et al., 2012), while the H_2 purity required for PEMFC should be more than 99.97% according to ISO 14687-2:2012. In contrast to the PSA, thermal swing adsorption (TSA) based on metal hydride (MH) could selectively react with H_2 by chemisorption and thus produces H_2 fuel with high purity up to more than 99.99% (Golmakani et al., 2017). Additionally, using the TSA instead of the PSA could improve the energy efficiency of the SOFC-PEMFC hybrid system from 59.4% to 63.7% without increasing the exergy destruction (Wu et al., 2018). Therefore, we further coupled the TSA with the water gas shift (WGS) to achieve a higher and more pure H_2 production, thus an SOFC-WGS-TSA-PEMFC hybrid system is developed for power generation (Wu et al., 2019a). It was found that the novel hybrid power system also has fast response within 20 s to reach a stable and energy efficient output. Consequently, the proposed SOFC-WGS-TSA-PEMFC hybrid system has demonstrated superior performance and has a promising potential for cleaner power generation which could run with different hydrocarbon fuel choices. Table 1 briefly summarizes the advantages and disadvantages of the above-mentioned hybrid fuel cell systems.

Table 1. The advantages and disadvantages of different hybrid fuel cell systems.

Hybrid fuel cell systems	Advantages	Disadvantages	References
Biomass-fed SOFC-Stirling engine-electrolyzer	High rate of hydrogen production (56.5 kg/day), low cost (41.76 $/GJ)	Low net electricity efficiency and exergy efficiency (26.51%)	Habidollahzade et al., 2018
SOFC-GT	High fuel flexibility (CH_4, natural gas, biogas, and so on), High overall cycle efficiency (>60%)	Low net electricity efficiency, power mismatch between SOFC and GT	Sghaier et al., 2018

CCHP consisting of SOFC, GT, CO_2 cycle, ORC, and LNG cold cycle	High overall exergy efficiency (>62.29%) due to cascade energy utilization, High CO_2 capture rate (79.2 kg/h)	Complicated system, high cost	Liu et al., 2019
SOFC-PSA-PEMFC	High overall exergy efficiency (61-63%), near zero emissions, car as power plant (CaPP) mode producing electricity, heat, and hydrogen	Low net electricity efficiency (42.5-45%), low hydrogen purity (<99.97%)	Fernandes et al., 2016
SOFC-WGS-TSA-PEMFC	High fuel flexibility (CH_4, natural gas, biogas, and so on), high energy efficiency (63.7%), fast transient response (<20 s), high hydrogen purity (>99.99%)	Complicated system	Wu et al., 2018, 2019a

However, the techno-economic performance of the hybrid power generation system with different hydrocarbon fuels is still unclear. The index of levelized cost of energy (LCoE) (Vazquez and Iglesias, 2015) is generally used for economy evaluation of an energy system. However, the thermo-economic model based on the index of the LCoE only takes the contributions of capital investment, investment interest, operation and maintenance fees into account. The LCoE model does not consider the contributions of the insurance and tax fees. In our previous work (Wu et al., 2019b), it was found that the insurance and tax fees contribute to approximately 10% of the annual cost for the hybrid fuel cell system. That is to say, the insurance and tax fees also play an important role in the thermo-economic performance, which

should be taken into account in the thermo-economic model. Therefore, this work introduces the economic index of specific electric energy cost (SEEC) to comprehensively evaluate the techno-economic performance for the proposed SOFC-WGS-TSA-PEMFC hybrid power generation system fed by different hydrocarbon fuels. The results help to obtain the development roadmap of the SOFC-WGS-TSA-PEMFC power generation technology, which is essential and valuable to stimulate the practical applications of this kind of hybrid system as distributed energy resource for clean power generation.

The composition structure of this paper is set as follows: In Section 2, the system description and working principle are first introduced. The system modeling including thermodynamics and thermo-economics modeling is presented in Section 3. Then, the influences of TSA working medium (different kinds of metal hydrides) and input fuel (four kinds of fuels) on the techno-economic performance of the hybrid system are analyzed and discussed. Finally, the corresponding development roadmap of this kind of hybrid power technology is demonstrated in detail under the current subsidy policy in Eastern China.

2. System description and working principle

In the SOFC-WGS-TSA-PEMFC hybrid electricity power generation system, the hydrocarbon fuel and air are pre-heated by the waste heat from the anode off-gas before they enter the SOFC component for power generation. In this work, four kinds of fuels including the NG, biogas, liquefied petroleum gas (LPG), and water gas are considered for the SOFC-WGS-TSA-PEMFC hybrid system. The SOFC anode off-gas then enters the two-stage WGS reactors for H_2 production, which includes the high-temperature (623 K) WGS for fast conversion reaction rate and the low-temperature (463 K) WGS for large amounts of H_2 conversion due to the exothermic reaction. Before entering the PEMFC for additional electricity power generation, the produced syngas from the WGS reactors enters the TSA reactor filled with MH to produce pure H_2 via reversible hydrogen absorption/desorption reactions. Herein, the reaction heat required for the H_2 desorption from the TSA reactor is taken from the waste heat of the WGS process by using heat exchangers, thus improving the thermal

efficiency of the hybrid system. The system description and the working principle of the hybrid system with the corresponding thermodynamic data are illustrated in Fig. 1.

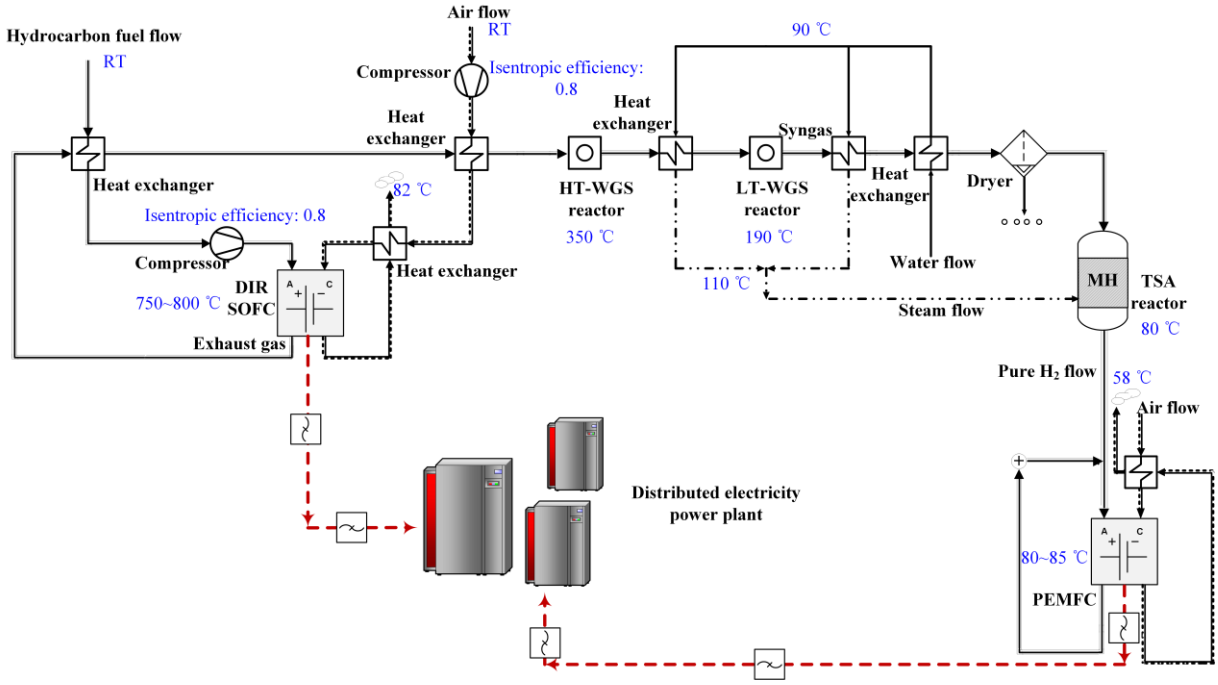

Fig. 1. System description and working principle of the proposed SOFC-WGS-TSA-PEMFC hybrid system for distributed electricity power generation (RT: room temperature).

3. System modeling

3.1. Thermodynamics modeling

The following assumptions are considered for the sake of simplifying the model.

1) All gases are approximated as ideal gas.
2) Pressure drops in the hybrid system's transportation pipelines are neglected.
3) No carbon deposition is assumed due to high steam to carbon ratio (Stiller et al., 2005).
4) Inside the SOFC, the reforming and electrochemical reactions are separately modeled.

Although the component CO of reformed gas can be used as the anode fuel for the electrochemical reaction with oxygen, the WGS reaction converting CO into H_2 always preferentially occurs in the presence of water.

5) Both the reforming and electrochemical reactions take place at equilibrium conditions (Aguiar et al., 2004). The temperature in the FCs is assumed to be stable during transient electrochemical process. This is because the temperature dynamics of the FCs can be neglected for the short time intervals which are corresponding to the response time of electrochemistry and fuel processor discussed in this work (Sedghisigarchi and Feliachi, 2004).

6) All the reactors are completely insulated, indicating no heat transfer between the reactors and environment.

The methane steam reforming (MSR) and WGS reactions occurring inside the SOFC can be described in Eqs. (1) and (2).

$$CH_4 + H_2O \rightarrow CO + 3H_2 \quad \Delta H = 206\ \text{kJ/mol} \tag{1}$$

$$CO + H_2O \rightarrow CO_2 + H_2 \quad \Delta H = -41\ \text{kJ/mol} \tag{2}$$

The corresponding MSR and WGS reaction equilibrium constant K_{MSR} and K_{WGS} is written as a function of reaction temperature, as shown below (Chan et al., 2002; Massardo and Lubelli, 2000).

$$\begin{aligned} K_{MSR} &= \frac{p_{CO} \cdot p_{H_2}^3}{p_{CH_4} \cdot p_{H_2O}} = f(T) \\ &= \exp(-2.63121\times10^{-11}\cdot T^4 + 1.24065\times10^{-7}\cdot T^3 - 2.25232\times10^{-4}\cdot T^2 + 0.195028\cdot T - 66.1395) \end{aligned} \tag{3}$$

$$\begin{aligned} K_{WGS} &= \frac{p_{CO_2} \cdot p_{H_2}}{p_{CO} \cdot p_{H_2O}} = f(T) \\ &= \exp(5.47301\times10^{-12}\cdot T^4 - 2.57479\times10^{-8}\cdot T^3 + 4.63742\times10^{-5}\cdot T^2 - 0.03915\cdot T + 13.2097) \end{aligned} \tag{4}$$

In the TSA reactor, the hydrogen desorption reaction kinetics of the MH can be described in Eq. (5), among which the expression of equilibrium pressure p_{eq} is written in Eq. (6). Herein, $\dot{m}_{TSA}$ (mol s^{-1}) is the H_2 flow velocity of desorption reaction, C_d (s^{-1}) and E_{act} (J mol^{-1}) stand for hydrogen desorption reaction rate constant and activation energy, respectively. ρ_{MH} (kg m^{-3}) and ρ_{HSA} (kg m^{-3}) are the density of saturated metal hydride and pure hydrogen storage alloy. a_n is the polynomial coefficient of $f(\frac{H}{M})$, where $\frac{H}{M}$ represents the hydrogen

storage capacity. Besides, ΔH_{TSA} (J mol^{-1}) is the reaction enthalpy of TSA process. T_{ref} is the reference temperature which is 273 K in this work. The main parameters for the TSA reaction based on AB_5-type MH used in these equations are listed in Table 2.

$$\dot{m}_{TSA} = C_d \cdot \exp(-\frac{E_{act}}{R_g T_{TSA}}) \cdot \left(\frac{p_g - p_{eq}}{p_{eq}} \right) \cdot (\rho_{MH} - \rho_{HSA}) \quad (5)$$

$$p_{eq} = \sum_{n=0}^{9} \left[a_n \cdot \left(\frac{H}{M} \right)^n \right] \cdot \exp\left[\frac{\Delta H_{TSA}}{R_g} \cdot \left(\frac{1}{T_{TSA}} - \frac{1}{T_{ref}} \right) \right] \quad (6)$$

Table 2. The main parameters for the TSA reaction based on AB_5-type MH used in Eqs. (5) and (6) (Jemni, 1999).

Parameters	Polynomial coefficients	Desorption rate constant, C_d (s^{-1})	Activation energy, E_{act} (kJ mol^{-1})	Gas pressure, p_g (bar)
Absorption	a_0=0.0075, a_1=15.2935, a_2=-34.577, a_3=39.9926, a_4=-26.7998, a_5=11.0397, a_6=-2.8416, a_7=0.446, a_8=-0.0391, a_9=0.0014	59.19	21.18	1
Desorption	a_0=-1.465, a_1=19.190, a_2=-42.086, a_3=49.087, a_4=-33.819, a_5=-14.437, a_6=-3.858, a_7=0.627, a_8=-0.0567, a_9=0.0021	9.57	23.88	0.085

The FC electrochemical reaction for electricity generation can be expressed in Eq. (7). The corresponding electrochemical models of SOFC and PEMFC are summarized in Table 3. The gross energy conversion efficiency and net electricity efficiency of the hybrid power system are respectively expressed in Eqs. (8) and (9). For the more detailed information about

the values of these parameters, please refer to our previous papers (Ni et al., 2007; Wu et al., 2019a).

$$H_2 + \frac{1}{2}O_2 \rightarrow H_2O(g) \quad \Delta H = -242\ \text{kJ/mol} \tag{7}$$

$$\eta_{Gross} = \frac{P_{SOFC} + P_{PEM}}{\varphi_{fuel} \cdot LHV_{fuel}} \tag{8}$$

$$\eta_{Net} = \frac{P_{SOFC} + P_{PEM} - P_{AUX}}{\varphi_{fuel} \cdot LHV_{fuel}} \tag{9}$$

Table 3. The electrochemical models of SOFC and PEMFC (Ferguson et al., 1996; Correa et al., 2004; Cheddie, 2010).

Parameter	Electrochemical equation
Cell voltage V_{cell}	$V_{cell} = E_N - V_{act} - V_{ohm} - V_{conc}$
Output power P_{FC}	$P_{FC} = \eta_{DC/AC} \cdot J \cdot A \cdot V_{cell}$
SOFC: equilibrium voltage $E_{N,SOFC}$, activation overvoltage $V_{act,SOFC}$, ohmic overvoltage $V_{ohm,SOFC}$, and concentration overvoltage $V_{conc,SOFC}$	$E_{N,SOFC} = 1.253 - 2.4516\times10^{-4} \cdot T_{SOFC} - \frac{R \cdot T_{SOFC}}{4F} \cdot \ln\left(\frac{p_{H_2O}^2}{p_{H_2}^2 \cdot p_{O_2}}\right)$ $V_{act,SOFC} = V_{act,SOFC,a} + V_{act,SOFC,c}$ $= \frac{R_g \cdot T_{SOFC}}{F} \cdot \ln\left[\frac{J}{2J_{0,a}} + \sqrt{\left(\frac{J}{2J_{0,a}}\right)^2 + 1}\right]$ $+ \frac{R_g \cdot T_{SOFC}}{F} \cdot \ln\left[\frac{J}{2J_{0,c}} + \sqrt{\left(\frac{J}{2J_{0,c}}\right)^2 + 1}\right]$ $V_{ohm,SOFC} = 2.99\times10^{-11} \cdot J \cdot l_e \cdot e^{\frac{10300}{T_{SOFC}}}$

$$V_{conc,SOFC} = V_{conc,SOFC,a} + V_{conc,SOFC,c}$$

$$= \frac{R \cdot T_{SOFC}}{2F} \cdot \ln\left(\frac{1 + \frac{R \cdot T_{SOFC} \cdot l_a \cdot J}{2F \cdot D_a^{eff} \cdot p_{H_2O}}}{1 - \frac{R \cdot T_{SOFC} \cdot l_a \cdot J}{2F \cdot D_a^{eff} \cdot p_{H_2}}} \right)$$

$$+ \frac{R \cdot T_{SOFC}}{4F} \cdot \ln\left(\frac{p_{O_2}}{\frac{p_c}{\delta_{O_2}} - \left(\frac{p_c}{\delta_{O_2}} - p_{O_2} \right) \cdot e^{\frac{R \cdot T_{SOFC} \cdot l_c \cdot J \cdot \delta_{O_2}}{4F \cdot D_c^{eff} \cdot p_c}}} \right)$$

PEMFC: equilibrium voltage $E_{N,PEM}$, activation overvoltage $V_{act,PEM}$, ohmic overvoltage $V_{ohm,PEM}$, and concentration overvoltage $V_{conc,PEM}$

$$E_{N,PEM} = 1.229 - 0.85 \times 10^{-3} \cdot (T_{PEM} - 298.15) + \frac{R \cdot T_{PEM}}{4F} \cdot \ln\left(p_{H_2}^2 \cdot p_{O_2} \right)$$

$$V_{act,PEM} = 0.948 - (0.00286 + 0.0002 \ln A + 4.3 \times 10^{-5} \cdot \ln \frac{p_{H_2}}{1.09 \times 10^6 \cdot e^{\frac{77}{T_{PEM}}}}) \cdot T_{PEM}$$

$$- 7.6 \times 10^{-5} \cdot T_{PEM} \cdot \ln \frac{p_{O_2}}{5.08 \times 10^6 \cdot e^{-\frac{498}{T_{PEM}}}} + 1.93 \times 10^{-4} \cdot T_{PEM} \cdot \ln I_{PEM}$$

$$V_{ohm,PEM} = I \cdot \left\{ \frac{181.6 \cdot \left[1 + 0.03 \cdot J + 0.062 \cdot \left(\frac{T_{PEM}}{303} \right)^2 \cdot J^{2.5} \right]}{\left(\psi - 0.634 - 3 \cdot J \cdot e^{4.18 \cdot \frac{T_{PEM} - 303}{T_{PEM}}} \right)} \cdot \frac{l_e}{A} + 0.0003 \right\}$$

$$V_{conc,PEM} = -B \cdot \ln\left(1 - \frac{J}{J_{\max}} \right)$$

The power consumption of the compressor (W_{comp}) is calculated in Eq. (10).

$$W_{\text{comp}} = \varphi \cdot Cp \cdot T_{in} \left(\gamma^{\frac{R}{Cp}} - 1 \right) \cdot \frac{1}{\eta_{ISE} \cdot \eta_{MEC}} \tag{10}$$

The energy equation over the heat exchanger can be described in Eq. (11).

$$\varphi_{\text{hot}} \cdot Cp_{\text{hot}} \cdot (T_{h1} - T_{l1}) = \varphi_{\text{cool}} \cdot Cp_{\text{cool}} \cdot (T_{h2} - T_{l2}) \tag{11}$$

3.2. Thermo-economics modeling

The following assumptions are considered for the sake of simplifying the thermo-economic model.

1）For the SOFC component, the cost of auxiliary devices including the combustor, mixers, and by-pass valves, is assumed as a fixed percentage 10% of the SOFC stack cost for simplification (Owebor et al., 2019; Samanta and Ghosh, 2017).

2） Since it is hard to quantitatively correlate the SOFC cost and the materials deterioration caused by high temperatures, the thermo-economic model of SOFC component does not consider the materials deterioration caused by the high temperatures.

3） The WGS reaction rate r is calculated with the assumption of a constant temperature over all the WGS reactor (Levenspiel, 1972).

4）According to the U.S. DOE (Department of Energy) target for the cycle life (1500 cycles or equivalent of 5000 operation hours) of solid-state hydrogen storage technology (U.S. DOE, 2015), each cycle duration t_{cycle} is assumed as the average value 3.33 h (≈5000 h/1500 cycles).

According to the system description of the SOFC-WGS-TSA-PEMFC hybrid electricity power generation system as illustrated in Fig. 1, the hybrid system mainly consists of the following components: SOFC, two-stages WGS, TSA based on MH, PEMFC, heat exchanger and compressor. The capital cost model of these components are described and summarized in Table A1, as shown in Appendix A. The total equipment capital cost C_{capt} of the hybrid system can be achieved by integrating all the components, as listed in Eq. (12).

$$C_{Capt} = C_{SOFC} + C_{PEM} + C_{HT-WGS} + C_{LT-WGS} + C_{TSA} + C_{Comp} + C_{HE} \quad (12)$$

The values of the important parameters shown in the capital cost equations are listed in Table A2, as shown in Appendix.

Besides the capital investment cost, the thermo-economic model also considers the annual operation cost C_{Oper}, the annual maintenance cost C_{Main}, the annual investment interest C_{Int}, the annual insurance C_{Ins}, and the tax per annum C_{Tax}. Herein, the capital cost can be also apportioned averagely as the annual depreciation cost C_{Depr} on the basis of cycle life. Table A3 shown in Appendix lists these annual cost models of the hybrid system. In this work, the SEEC (CNY/kW h) is used as the techno-economic index to comprehensively evaluate the economy

of the SOFC-WGS-TSA-PEMFC hybrid system, which is written in Eq. (13). The flowchart of the thermo-economic modeling procedure is summarized in Fig. 2.

$$SEEC = \frac{C_{\mathrm{Depr}} + C_{\mathrm{Oper}} + C_{\mathrm{Main}} + C_{\mathrm{Int}} + C_{\mathrm{Ins}} + C_{\mathrm{Tax}}}{(W_{\mathrm{SOFC}} + W_{\mathrm{PEM}}) \cdot t_{\mathrm{oper}} / \lambda} \tag{13}$$

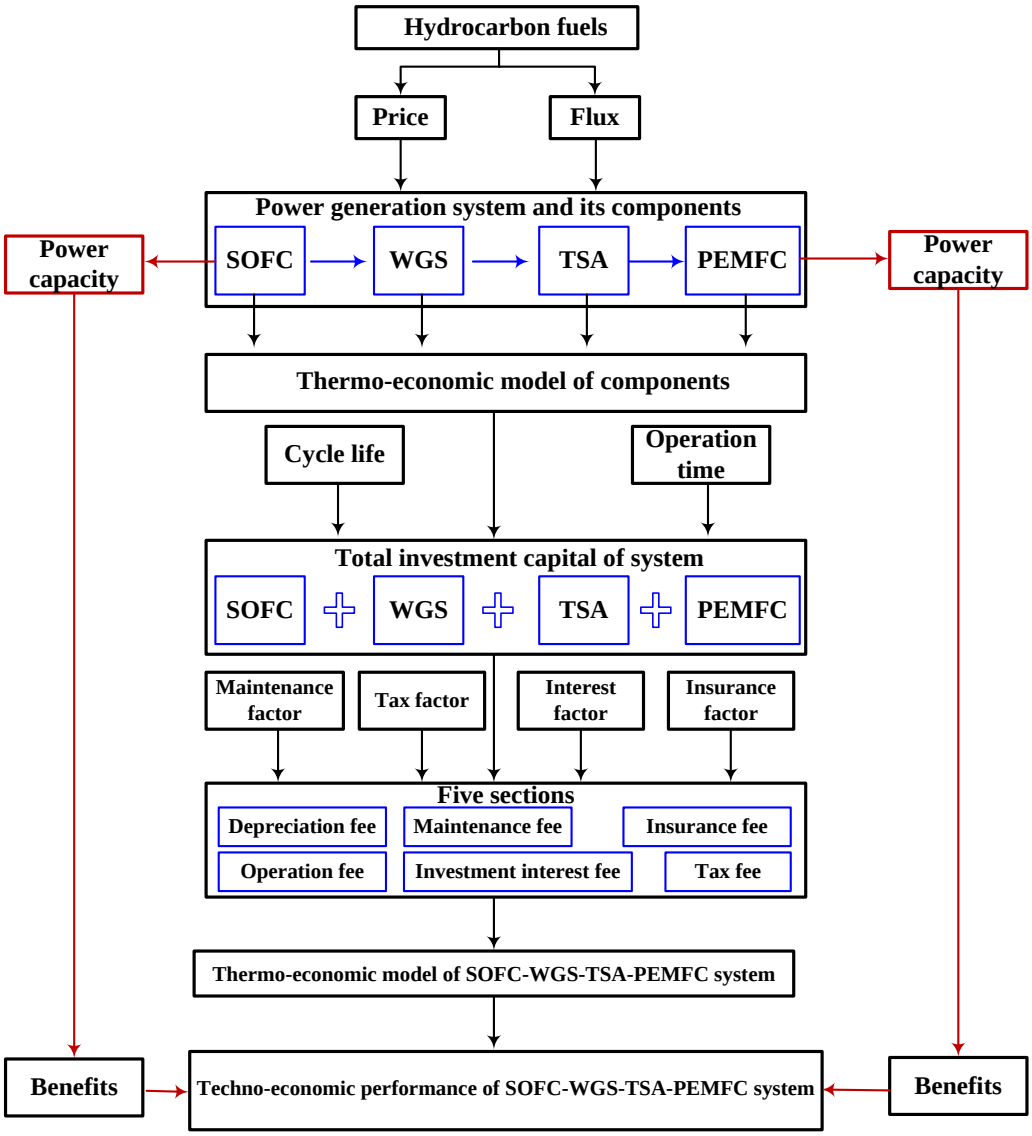

Fig. 2. Flowchart of the thermo-economic modeling procedure of the proposed SOFC-WGS-TSA-PEMFC power system.

4. Results and discussion

4.1. Techno-economic analysis using different kinds of MH as TSA working medium

In the SOFC-WGS-TSA-PEMFC hybrid system, the TSA unit aims to purify H_2 and prevent gas impurities from poisoning the expensive anodic-catalyst Pt of the PEMFC, thus ensuring a long operating lifetime. Therefore, the TSA component plays an important role in the techno-economic analysis of the hybrid system for electricity power generation. Herein, the widely used MHs are selected as the TSA working medium, which are AB_5-type $LaNi_5$, AB-type TiFe, and A_2B-type Mg+2wt%Ni, respectively. The hydrogen absorption/desorption characteristics of these MHs are summarized in Table 4.

Table 4. The hydrogen absorption/desorption characteristics of AB_5-type, AB-type, and A_2B-type MHs.

MHs		Density (kg/m^3)	Price (million CNY/ton)	Capacity (wt%)	Cycles
AB_5-type	$LaNi_5$[a]	8400	0.35	1.390	18180
	$MmNi_{4.6}Al_{0.4}$[b]	8400	0.26	1.150	18180
A_2B-type Mg+2 wt% Ni[c]		1740	0.019	7.480	1500
AB-type TiFe[d]		5930	0.012	1.875	1500

a: Tarasov et al., 2018; b: Muthukumar et al., 2005; c: Reiser, 2000; d: Bellosta von Colbe et al., 2019; Fiori et al., 2015

Fig. 3 shows the techno-economic performance of an NG-fed SOFC-WGS-TSA-PEMFC hybrid system with 10 MWe output under different types of MHs as the TSA working medium. Clearly, selecting different MHs massively influences the unit H_2 production cost (UHPC) to vary in a large range of 0.983~4.220 CNY/kg H_2 while the SEEC varies in a small range of 0.462~0.468 CNY/kW h. Among the three kinds of MHs, the typical AB_5-type $LaNi_5$ results in the largest SEEC (0.468 CNY/kW h) and UHPC (4.220 CNY/kg H_2) for the hybrid system. This is mainly because $LaNi_5$ has a very high market price (0.35 million CNY/ton) and relatively small hydrogen capacity (1.390 wt%), which is caused by expensive and heavy rare earth metals involved in $LaNi_5$. Compared with the typical AB_5-type MH, the AB-type TiFe and A_2B-type Mg+2wt%Ni have higher hydrogen capacities and the lower market prices

(shown in Table 4), and these characteristics help to reduce the UHPC by approximately 60% and 77%, respectively.

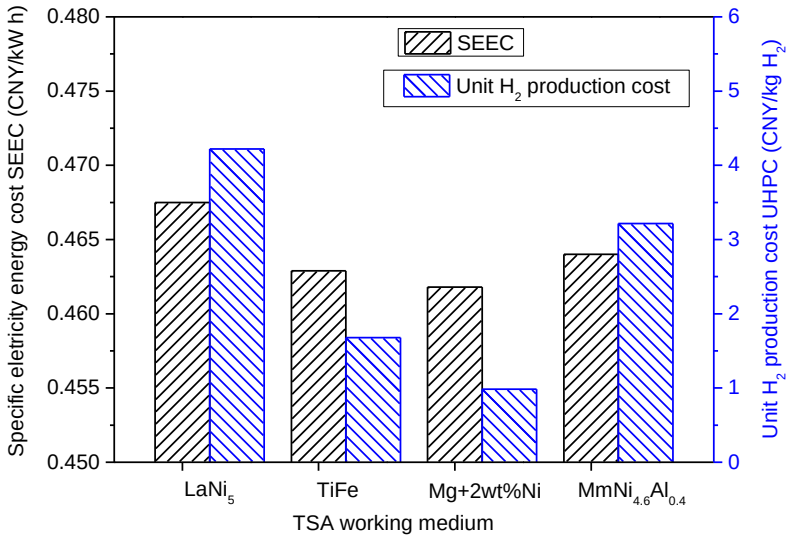

Fig. 3. The economic comparison of the SOFC-WGS-TSA-PEMFC hybrid electricity power generation system using different MHs as the TSA working medium.

Although the selection of MHs has a large impact on the economy of H_2 production for the PEMFC, its impact on the economy for electricity power generation is very small. For instance, the SEEC can be reduced by a maximum of 1.3% by replacing Mg+2wt%Ni for $LaNi_5$ as the MH. The main reason is that the TSA component contributes to a small portion of the total capital investment cost for the 10MWe SOFC-WGS-TSA-PEMFC hybrid system. Table 5 lists the capital investment costs of each primary component of the hybrid system with the three different types of MHs. Clearly, the SOFC and the PEMFC, as the power generation components, contribute to the most of the total capital investment cost, while the TSA component who is responsible for H_2 production for the PEMFC has a small contribution of at most 6.3%. In such a 10 MWe hybrid system, the component cost of the SOFC, PEMFC, TSA, WGS, and the auxiliary devices (compressor and heat exchanger) are calculated to be 42.28 million CNY (63.7%), 13.36 million CNY (20.1%), 4.21 million CNY (6.3%), 3.57 million CNY (5.4%), and 2.93 million CNY (4.4%), respectively. With TiFe and Mg+2wt%Ni as the

MHs, the contribution of the TSA component further reduces to 2.21% and 1.11%, as shown in Fig. 4a. In the TSA component, the cost of MH material dominates the TSA cost because its cost distribution ratio is more than 75%. In the case of $LaNi_5$ MH as the working medium, the cost ratio reaches up to 99%, indicating that the MH price determines the capital investment cost of the TSA component.

Table 5. The capital investment cost of each primary component of the NG-fed SOFC-WGS-TSA-PEMFC hybrid system with different types of MH.

Components	SOFC	PEMFC	WGS	TSA				Auxiliary devices	
				$LaNi_5$	$MmNi_{4.6}Al_{0.4}$	TiFe	Mg+2wt% Ni	Compressor	Heat exchanger
Capital cost (million CNY)	42.28	13.36	3.57	4.21	3.19	1.40	0.70	0.75	2.18

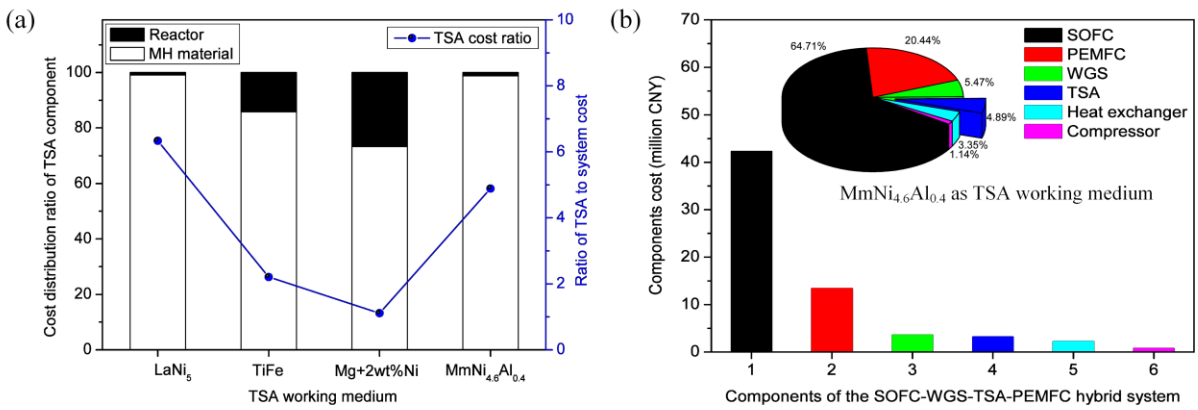

Fig. 4. (a) The effects of different MHs on the TSA component cost; (b) The components cost and their cost distribution of the hybrid system using $MmNi_{4.6}Al_{0.4}$ as the MH.

Since the TSA component cost has a small effect on the overall system's SEEC, the selection of the MH should preferentially be based on the feasibility and operability of the MH technology as the TSA for H_2 production. Although the AB-type TiFe and A_2B-type Mg+2wt%Ni have the lower price and the higher hydrogen capacity, these two types of MHs have other practical disadvantages. For example, the hydrogen absorption/desorption reactions of TiFe are very difficult to activate thermodynamically, thus it is immature to achieve large-scale synthetization. For the Mg+2wt%Ni, the hydrogen absorption/desorption reactions can

only be initiated at high temperatures (Reiser, 2000), indicating that an extra heating/cooling equipment will be required. An auxiliary heat exchanger is also needed to recycle the waste heat, even though a large amount of waste heat appear in the hybrid system. The additional devices will inevitably increase the auxiliary components investment cost and the system complexity. For comparison, the typical AB_5-type MH has been widely applied in the commercial applications due to the advantages of easy activation, mild operating pressure and temperature (close to normal pressure and temperature), mature large-scale synthetization technology, and stable hydrogen absorption/desorption cycles (Panwar and Srivastava, 2018; Srivastava and Upadhyaya, 2011). The highest hydrogen absorption/desorption lifetime cycles of the AB_5-type MH is reported to be as high as 18180 cycles (Tarasov et al., 2018), which is over 10 times larger than those of AB- and A_2B-type MHs. In fact, the ultra-long cycle life can remedy the high MH cost to some extent, thus reducing the capital investment cost of the TSA component. In addition, the cheaper AB_5-type $MmNi_{4.6}Al_{0.4}$ MH can be used to substitute the $LaNi_5$ to further reduce the cost by utilizing a misch metal rather than the expensive pure rare earth metal La. When the $MmNi_{4.6}Al_{0.4}$ is used as the TSA working medium, the SEEC of the NG-fed 10 MWe SOFC-WGS-TSA-PEMFC hybrid system is reduced to 0.464 CNY/kW h. The corresponding components cost and their cost distribution are demonstrated in Fig. 4b. Consequently, the modified AB_5-type $MmNi_{4.6}Al_{0.4}$ is suggested to be the TSA working medium for large-scale electricity power generation in the practical applications. It is noted that the following hybrid systems adopt the $MmNi_{4.6}Al_{0.4}$ MH as the TSA working medium.

4.2. Techno-economic analysis using different fuels

4.2.1. Natural gas

Since the NG refueling infrastructure has been well-established in China, the techno-economic performance of the NG-fed SOFC-WGS-TSA-PEMFC hybrid system is first evaluated. The NG composition is 85% CH_4, 7% C_2H_6, 2% C_3H_8, 5% CO_2, and 1% N_2, whose latest price (July 2019) in Shanghai, China is 3250 CNY/ton. As seen in Fig. 3, the SEEC and UHPC of the NG-fed 10 MWe hybrid system are calculated to be 0.464 CNY/kW h and 3.216 CNY/kg H_2, respectively. Since the economic index of the LCoE (expressed in Eq. (14)) is

generally adopted for economy evaluation from the point of energy generation, the LCoE results have been proven to reasonably reflect the thermo-economic performance of the energy generation systems (Cruz et al., 2017; Kuckshinrichs and Koj, 2018; Barutha et al., 2019). Therefore, we further compared the SEEC results with the most commonly used LCoE method for the validation of the proposed thermo-economic model to ensure the accuracy of the simulations. It was found that the calculated LCoE value of the 10 MWe NG-fed SOFC-WGS-TSA-PEMFC hybrid power system proposed in this work is 0.478 ¢/kW h, which is comparable to the SEEC value (0.464 CNY/kW h) for the same energy system. The good agreement between the SEEC and the LCoE values indicates that the proposed thermo-economic model based on the SEEC is reasonable and accurate for the comprehensive economy evaluation of the SOFC-PEMFC hybrid system.

$$LCoE = \frac{C_{\mathrm{Capi}} \cdot \dfrac{f_{\mathrm{Int}} \cdot (1+f_{\mathrm{Int}})^{\lambda}}{(1+f_{\mathrm{Int}})^{\lambda}-1} + C_{\mathrm{Oper}} + C_{\mathrm{Main}}}{(P_{\mathrm{SOFC}} + P_{\mathrm{PEM}}) \cdot t_{\mathrm{oper}} / \lambda} \tag{14}$$

Generally, the annual cost of the NG-fed SOFC-WGS-TSA-PEMFC hybrid system consists of the operation, depreciation, investment interest, maintenance, insurance, and tax, as shown in Fig. 5a. Herein, the total capital investment cost of the hybrid system is allocated to the depreciation expense during the operating life time of 10 years. It can be found that the operation and depreciation fees contribute to the majority of the annual cost, accounting for 77.47% and 16.07%, respectively. This is because that a large amount of NG with the flux of about 29 ton per day is required to input into the hybrid system for the power generation of 10 MWe, which results in the high operation fee. The majority of the contribution suggests that, besides initial capital investment, the techno-economic performance of the NG-fed hybrid system for distributed power generation mainly depends on the price of the NG fuel.

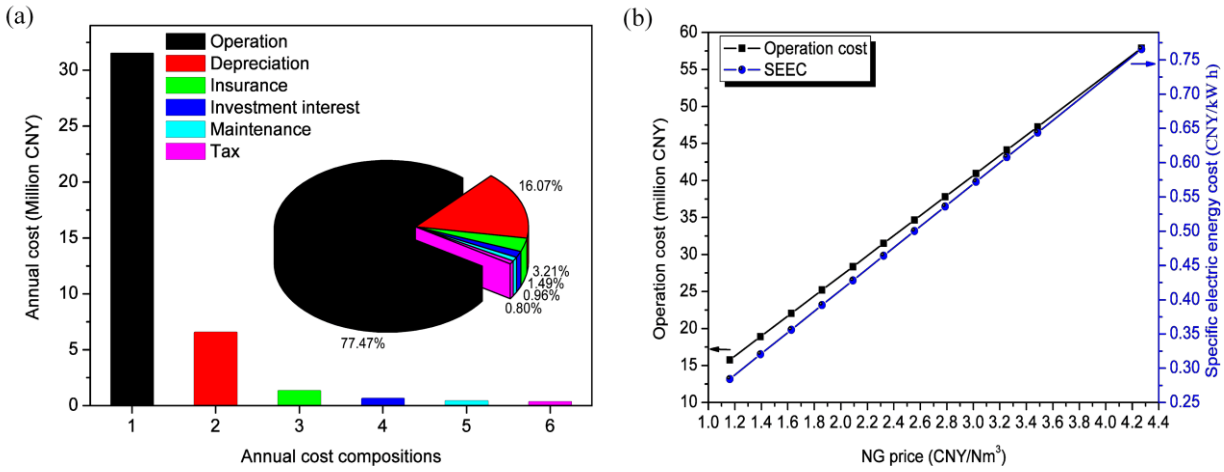

Fig. 5. Techno-economic performance of the NG-fed SOFC-WGS-TSA-PEMFC hybrid system. (a) The annual cost compositions and their cost distribution; (b) The sensitivity analysis of the hybrid system to the NG price.

On the other hand, the NG price often fluctuates in the market. Therefore, the effect of the fluctuation of NG price on the techno-economic performance of the hybrid system is further investigated to estimate the market sensitivity. Fig. 5b displays the operation cost and the SEEC of the NG-fed hybrid system at different NG prices. When the NG price increases from 1.161 to 3.484 CNY/Nm^3, the annual operation cost increases from 15.75 to 47.26 million CNY. Accordingly, the SEEC of the hybrid system is increased from 0.284 to 0.644 CNY/kW h. With the NG price fluctuation of 20%, the SEEC presents a smaller variation of 15%. At a higher fluctuation of 50%, a variation of 38% occurs in the SEEC. The smaller variation indicates that the NG-fed hybrid system has a relatively low sensitivity to the market fluctuation of the NG price. In addition, the SEEC increases to 0.7656 CNY/kW h at a high NG price of 4.270 CNY/Nm^3, which is comparable to the present on-grid electricity cost (0.7655 CNY/kW h) of distributed electricity power plant fed by NG in Shanghai, China (SparX, 2018).

Actually, the NG is a kind of regional energy, suggesting that NG prices may be different around the world. Taking New York of USA as an example, the latest NG price (2 August 2019) is 2.07 $/mmbtu (0.503 CNY/Nm^3) (U.S. Energy Information Administration, 2019), which is much cheaper than the NG price in China. This is because that the national energy consumption structure in China is rich coal, deficient oil, and lean NG. Statistically,

approximately 61.4 billion NG needs to be imported into China and 32% of the NG resource depends on the import trade in 2015 (China, 2016). Therefore, it is significant to develop other fuels for the SOFC-WGS-TSA-PEMFC hybrid system to generate power at a large-scale, which is in line with the national conditions of energy structure in China. In this context, the techno-economic performance of the hybrid system fueled by biogas, liquefied petroleum gas, and water gas is further evaluated in this work.

4.2.2. Biogas

Biogas is an important potential resource as the alternative fuel of NG. It can be stored and transported to the user by NG pipelines or gas tanks with well-established infrastructure for practical applications. This is because that the main component of the biogas is also methane. Herein, the biogas is assumed to have a composition of 60% CH_4 and 40% CO_2 in the techno-economic model. It was recently reported that, excluding the initial investment, the average cost of biogas is 0.11 \$/Nm^3, and the selling price is 0.22 \$/Nm^3 (1.512 CNY/Nm^3) in China (Xiong et al., 2011), which is cheaper than the NG. In addition, the biogas-fed SOFC-WGS-TSA-PEMFC hybrid system presents a high overall energy conversion efficiency up to 63.5%, which is comparable to the efficiency (64%) of the NG-fed hybrid system (Wu et al., 2018). The detailed performance of the biogas-fed SOFC-WGS-TSA-PEMFC hybrid system for distributed electricity power generation is summarized in Table 6. The SEEC of the biogas-fed 10 MWe hybrid electricity power generation system is calculated to be 0.469 CNY/kW h, which is slightly higher than that of the NG-fed hybrid system with the same level of power output.

Table 6. The energetic and economic performance of the biogas-fed SOFC-WGS-TSA-PEMFC hybrid system for distributed electricity power generation.

Parameters	Biogas flux (kg/s)	Power (kW)		Biogas LHV (MW)	Auxiliary power (kW)	Net electricity efficiency	SEEC (CNY/kW h)
		SOFC	PEMFC				
Values	0.824	8776.27	1223.76	14.57	741.22	63.5%	0.469

Fig. 6a and 6b reveal the components cost and the annual cost of the biogas-fed SOFC-WGS-TSA-PEMFC hybrid system with 10 MWe electricity power, respectively. The SOFC and PEMFC, which are all the electricity power generation components, contribute to about 87% of the total capital investment cost of the biogas-fed hybrid system. On the other hand, the gas processing units, WGS and TSA, account for 7.55%, among which the TSA has the lower proportion (3.02%) compared with that of an NG-fed hybrid system (4.89%). The reduction in the proportion of the TSA unit cost is mainly attributed to the reduced amount of the TSA working medium MH required to produce H_2 for the PEMFC. In the NG-fed hybrid system, the amount of H_2 production by TSA is 0.265 mol/min for the PEMFC power generation of 2063 kW. By comparison, the amount of H_2 production in the biogas-fed system is 0.158 mol/min for the PEMFC power of 1224 kW. Therefore, the NG-fed hybrid system needs more MH material to produce more H_2 for the PEMFC. As mentioned above, the cost of the TSA unit cost consists of the MH cost C_{MH} and the reactor cost C_{reac}. Additionally, the MH cost accounts for the most of the TSA unit cost, which is confirmed by the MH cost ratio up to 99% in the case of $LaNi_5$ MH as the working medium. Therefore, including more MH material leads to higher TSA unit cost, and this causes the TSA cost in the NG-fed system with more H_2 production and additional MH material to be higher than that of the biogas-fed system. In the annual cost composition, the operation fee also occupies the majority (78.38%) of the annual cost. Moreover, the proportion of annual operation fee is higher when compared with the NG-fed hybrid system, indicating the significance of the biogas fuel in the techno-economic performance of the SOFC-WGS-TSA-PEMFC hybrid system. The comparison of the effect of price fluctuation of different fuels on the SEEC of the hybrid system is demonstrated in Fig. 7a. For the biogas fuel, the price fluctuation of 20% and 50% leads to the variation of 15.7% and 39.2% in the SEEC, which are higher than the case involving NG fuel. The comparison suggests that the biogas-fed SOFC-WGS-TSA-PEMFC hybrid system is more sensitive to market prices than the NG-fed counterpart. The main reason for the more sensitivity is that the proportion (78.38%) of operation fee in the annual cost for the biogas-fed hybrid system is higher than the value (77.47%) of the NG-fed counterpart. In addition, the effects of different market price factors' fluctuation on the SEEC of the biogas-fed SOFC-WGS-TSA-PEMFC

hybrid system are further analyzed and illustrated in Fig. 7b. Herein, eight kinds of market price factors are considered, which are the prices of 316L steel, PEMFC catalyst, MH, WGS catalyst, tax, interest, insurance, and biogas fuel. It can be seen that the SEEC of the hybrid power system is sensitive to only the fluctuation of the biogas price, while the other seven kinds of market price factors present little effect (no more than 1%) on the SEEC. Because biogas price usually has a low fluctuation in the market, it can be concluded that the proposed SOFC-WGS-TSA-PEMFC hybrid system is lowly sensitive to the market price fluctuation.

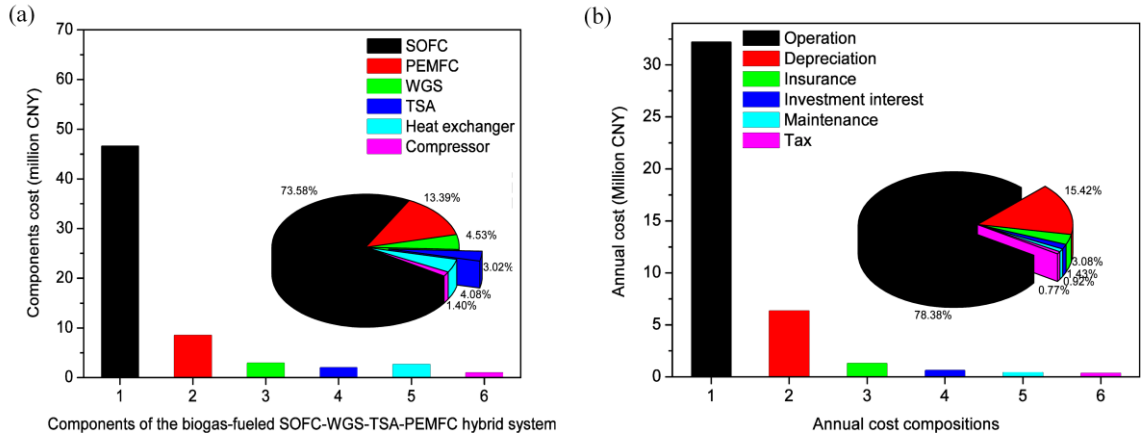

Fig. 6. Techno-economic performance of the biogas-fed SOFC-WGS-TSA-PEMFC hybrid system. (a) The components cost compositions and their cost distribution; (b) The annual cost compositions and their cost distribution.

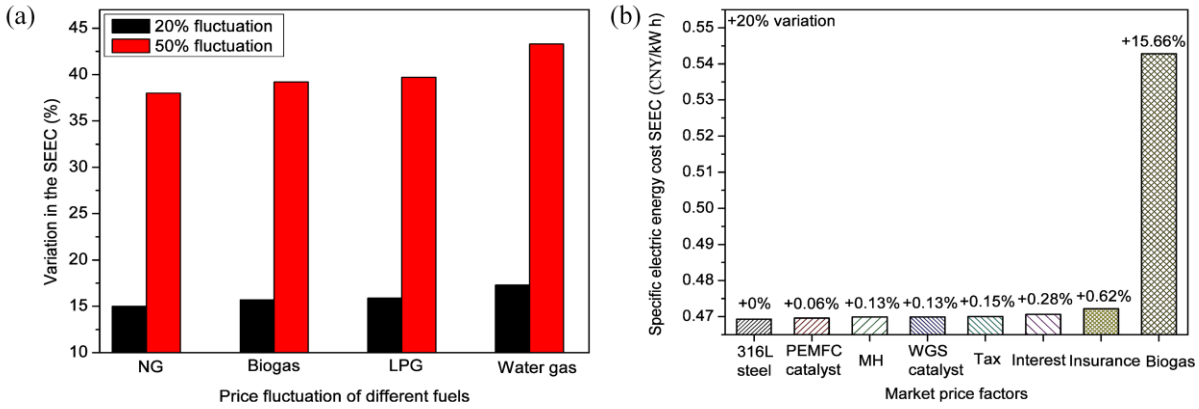

Fig. 7. Sensitivity analysis of the hybrid systems fed by different fuels to market price fluctuation. (a) The comparison between four different fuels; (b) The effects of different market price factors' fluctuation on the SEEC.

4.2.3. Liquefied petroleum gas

LPG is another important fuel that has been widely used in the practical applications. Its infrastructure is also well established in China. LPG is comprised of 40% C_3H_8 and 60% C_4H_{10}. The latest price of the LPG (July 2019) in Shanghai, China is 3500 CNY/ton, and its LHV reaches up to 45.7 MJ/kg, both of which are a little higher than those of the NG.

When using LPG as the input fuel of the SOFC-WGS-TSA-PEMFC hybrid system for power generation, the LPG compositions C_3H_8 and C_4H_{10} first undergo direct internal reforming reactions to be converted into CO and H_2 inside the SOFC in the presence of steam. Then, CO further reacts with H_2O via WGS reaction to produce more H_2 as the anode fuel of SOFC. Although the reformed gas component CO can be used as the anode fuel to be consumed, the WGS reaction converting CO into H_2 always preferentially occurs in the presence of water. Eqs. (15-17) describe the reaction equations of steam reforming of propane (PSR) and butane (BSR) as well as the WGS, respectively.

$$C_3H_8 + 3H_2O \rightarrow 3CO + 7H_2 \quad \text{PSR}, \Delta H = 499\ \text{kJ/mol} \tag{15}$$

$$C_4H_{10} + 4H_2O \rightarrow 4CO + 9H_2 \quad \text{BSR}, \Delta H = 651\ \text{kJ/mol} \tag{16}$$

$$CO + H_2O \rightarrow CO_2 + H_2 \quad \Delta H = -41\ \text{kJ/mol} \tag{17}$$

For the reforming reactions, the components of the reaction products (gas mixture) and their concentrations closely depend on the reaction equilibrium constant *K*, which is a function of reaction temperature only. Fig. 8 shows the polynomial fitting curves of the reaction equilibrium constant of the PSR and BSR at different temperatures on the basis of the experimental data (Cui and Kær, 2018). It is shown that the polynomial fitting agrees well with the experimental data. Therefore, the function between the temperature and the equilibrium constant can be written in Eq. (18) and Eq. (19) for the PSR and BSR, respectively. When the reforming temperature reaches up to 1023 K (the SOFC operating temperature in this study), the reaction equilibrium constant of the PSR and BSR is as high as 6.7×10^{11} and 3.6×10^{16}. The extremely high reaction equilibrium constant suggests that the reforming reaction is completely

finished. Therefore, the compositions C_3H_8 and C_4H_{10} of the LPG are assumed to be completely converted into CO and H_2 in this work. The gas compositions after the reforming and WGS reactions of the LPG are comprised of 13.35% CO, 55.25% H_2, 7.58% CO_2, and 23.83% H_2O with the S/C ratio of 2.5.

$$K_{PSR} = \frac{p^3_{CO} \cdot p^7_{H_2}}{p_{C_3H_8} \cdot p^3_{H_2O}} = f(T) \tag{18}$$
$$= \exp(-1.224\times10^{-10}\cdot T^4 + 5.613\times10^{-7}\cdot T^3 - 0.001\cdot T^2 + 0.886\cdot T - 290.91)$$

$$K_{BSR} = \frac{p^4_{CO} \cdot p^9_{H_2}}{p_{C_4H_{10}} \cdot p^4_{H_2O}} = f(T) \tag{19}$$
$$= \exp(-1.921\times10^{-10}\cdot T^4 + 8.421\times10^{-7}\cdot T^3 - 0.00145\cdot T^2 + 1.224\cdot T - 389.54)$$

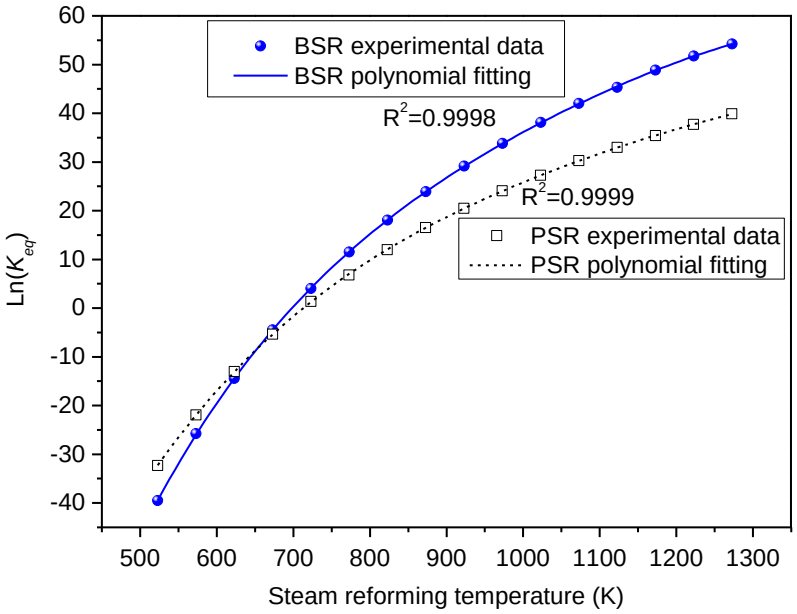

Fig. 8. The polynomial fitting curves of the reaction equilibrium constant of the PSR and BSR at different temperatures.

Table 7 lists the energetic and economic performance of the 10 MWe SOFC-WGS-TSA-PEMFC hybrid system using LPG as the fuel. Clearly, the net electricity efficiency of the LPG-fed hybrid system is 55.33%, which is much lower than those of NG- and biogas-fed hybrid systems. Accordingly, the SEEC of the LPG-fed 10 MWe hybrid system reaches up to 0.511 CNY/kW h, which is higher than those of the NG- and biogas-fed hybrid systems. The lower

energy efficiency and the higher electricity generation cost signify that the LPG-fed SOFC-WGS-TSA-PEMFC hybrid system may not be suitable as the distributed electricity power plant.

Table 7. The energetic and economic performance of the LPG-fed SOFC-WGS-TSA-PEMFC hybrid system for distributed power generation.

Parameters	LPG flux (kg/s)	Power (kW)		LPG LHV (MW)	Auxiliary power (kW)	Net electricity efficiency	SEEC (CNY/kW h)
		SOFC	PEMFC				
Values	0.322	8773.87	1227.15	14.74	1845.12	55.33%	0.511

The components cost and annual cost of the LPG-fed SOFC-WGS-TSA-PEMFC hybrid system with 10 MWe electricity power are illustrated in Fig. 9. Herein, the electricity generation components SOFC and PEMFC account for about 84% of the total capital investment cost, while the gas processing unit (WGS and TSA components) cost have been reduced to 5.7% compared with the NG- and biogas-fed hybrid system. Accordingly, the proportion of auxiliary unit (compressor and heat exchanger) is increased to 10.3% due to the significantly increased compression work (1845.12 kW). The comparison indicates that the cost of H_2 production and purification processes has become lower in the LPG-fed hybrid system. This is mainly because that the SOFC anode off-gas is a lean not rich fuel containing H_2 and CO, whose composition is 7.42% H_2, 1.53% CO, 19.40% CO_2, and 71.65% H_2O. Most of the H_2 and CO after the DIR are consumed in the SOFC component, causing the highest proportion of about 71% for the SOFC component cost. In the annual cost composition, the operation fee is also increased to near 80% because of the higher fuel price of LPG over NG and biogas fuels. The effect of the LPG price fluctuation on the SEEC of the SOFC-WGS-TSA-PEMFC distributed hybrid system is illustrated and compared in Fig. 7a, whose variations in the SEEC are accordingly increased to about 16% and 40% with the LPG price fluctuation of 20% and 50%, respectively.

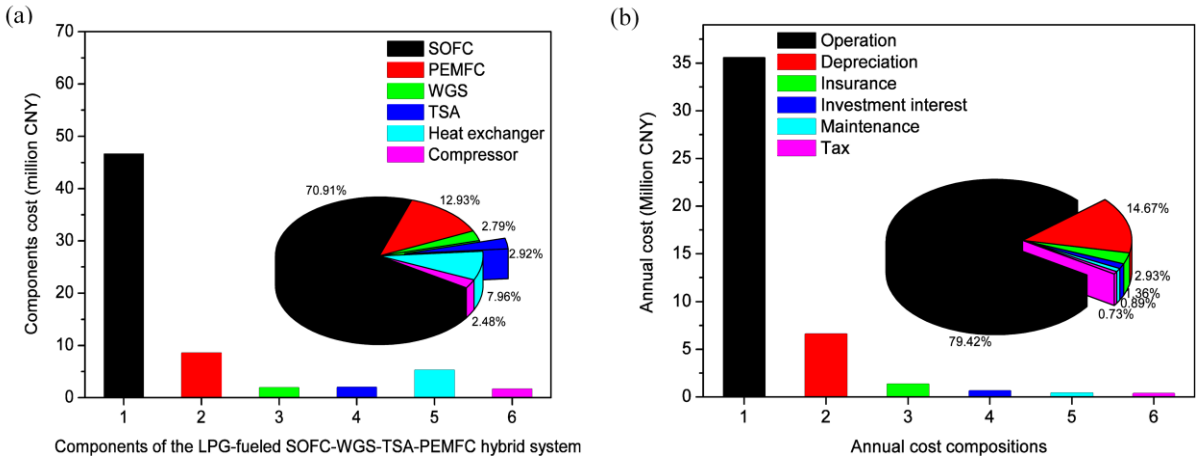

Fig. 9. Techno-economic performance of the LPG-fed SOFC-WGS-TSA-PEMFC hybrid system. (a) The components cost compositions and their cost distribution; (b) The annual cost compositions and their cost distribution.

4.2.4. Water gas

Water gas, consisting of 50% H_2, 40% CO, 5% CO_2, and 5% N_2, can be also used as the fuel of the SOFC-WGS-TSA-PEMFC hybrid system. Its price is the lowest among the other fuel options, which is 1.3 CNY/Nm^3 in Shanghai, China in 2015. However, the water gas has a low LHV, which is 10.05~10.87 MJ/Nm^3. Table 8 lists the energetic and economic performance of the 10 MWe water gas-fed SOFC-WGS-TSA-PEMFC hybrid system. According to this, the water gas-fed hybrid system has the lowest net electricity efficiency and the highest electricity generation cost, strongly indicating that the water gas is not a promising fuel for the hybrid system. The main reason for the lowest net electricity efficiency and the highest electricity generation cost is due to the relatively low LHV of water gas. Actually, the LHV (10.05~10.87 MJ/Nm^3) of the water gas is the lowest. By comparison, the LHV of the NG, biogas, and LPG is 34.9 MJ/Nm^3, 12 MJ/kg (~13.2 MJ/Nm^3), and 45.7 MJ/kg (~107 MJ/Nm^3), respectively. The lowest LHV of the water gas causes the largest fuel gas flux (1.276 kg/s) for the same power output of the SOFC-WGS-TSA-PEMFC hybrid system, which is much more than the NG flux (0.341 kg/s), the biogas flux (0.824 kg/s), and the LPG flux (0.322 kg/s). In general, the larger fuel gas flux indicates higher power consumption by compression. It is because that the larger fuel gas flux usually needs more oxygen for the electrochemical

reaction inside the SOFC to take place. Before entering the SOFC, the anode and cathode fuel gas should go through the compressor to elevate the temperature and pressure, as illustrated in Fig. 1. According to Eq. (10), the power consumption W_{comp} of the compressor is proportional to the input fuel gas flux φ. Therefore, the larger gas flux results in the more power consumption in the compression process. Consequently, the consumed auxiliary power (~1940 kW) is the largest for the water gas fed SOFC-WGS-TSA-PEMFC hybrid system, which is more than twice as large as the value (~741 kW) of biogas-fed hybrid system. That's also why the water gas fed hybrid power generation system has the lowest net electricity efficiency. Besides, the lowest net electricity efficiency and the largest fuel flux inevitably lead to the highest electricity generation cost for the case of water gas. These observations also explain why water gas has been out of the market in Shanghai since 2016.

Table 8. The energetic and economic performance of the water gas-fed SOFC-WGS-TSA-PEMFC hybrid system for distributed power generation.

Parameters	Water gas flux (kg/s)	Power (kW)		Water gas LHV (MW)	Auxiliary power (kW)	Net electricity efficiency	SEEC (CNY/kW h)
		SOFC	PEMFC				
Values	1.2764	8776.68	1223.75	18.90	1940.75	42.65%	0.785

Fig. 10 shows the components cost and the annual cost of the water gas-fed SOFC-WGS-TSA-PEMFC hybrid system with 10 MWe electricity power. Clearly, the water gas-fed hybrid system has a similar cost distribution to the LPG-fed system. The unit SOFC and PEMFC costs are calculated to be 5307 and 6924 CNY/kW h, respectively. The higher unit cost of the PEMFC is mainly attributed to the use of noble metal Pt as the catalyst. The big difference between the water gas and the other fuels is that the operation fee is remarkably increased to 59 million CNY, which is more than 1.5 times as large as those of the other fuels. Accordingly, in comparison to other fuel options, the water gas-fed hybrid system is the most sensitive to the market price fluctuation of the fuel, as can be seen in Fig. 7a.

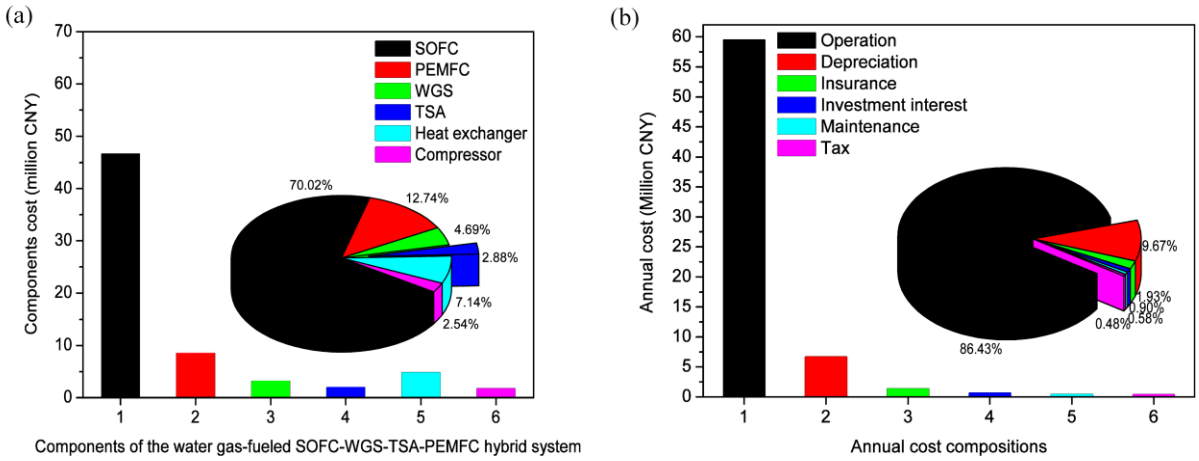

Fig. 10. Techno-economic performance of the water gas-fed SOFC-WGS-TSA-PEMFC hybrid system. (a) The components cost compositions and their cost distribution; (b) The annual cost compositions and their cost distribution.

4.3. Technology roadmap of the SOFC-WGS-TSA-PEMFC hybrid system with different fuels for distributed electricity power generation in Eastern China

The energy conversion and economic performance of the SOFC-WGS-TSA-PEMFC hybrid system fed by different fuels such as NG, biogas, LPG and water gas are separately evaluated in the above-mentioned analyses and discussion. The comparison between the four fuel options is further conducted in this paper, thus to achieve the development roadmap of the SOFC-PEMFC distributed power generation technology.

Fig. 11 illustrates the comparison of techno-economic performance between the SOFC-WGS-TSA-PEMFC hybrid system with different fuels. Clearly, the NG- and biogas-fed hybrid systems have the highest net electricity efficiency (63.5%~64%) among the discussed hybrid systems. For comparison, the efficiency of the LPG- and water gas-fed hybrid systems is much lower, which is 55.33% and 42.65%, respectively. Accordingly, the higher efficiency leads to the lower SEEC for the hybrid system. The NG- and biogas-fed hybrid systems present the lowest SEEC (0.464~0.469 CNY/kW h), while the LPG- and water gas-fed hybrid systems have the SEEC values as high as 0.511~0.785 CNY/kW h. Although the LPG has a much higher price than the water gas, the electricity power generation cost of the LPG-fed hybrid

system is much lower, because LPG has a higher heat value of over four times larger than that of water gas. In consequence, the higher efficiency and lower electricity power generation cost strongly reveal that the NG and biogas are the cost-optimal fuels for the SOFC-WGS-TSA-PEMFC hybrid system.

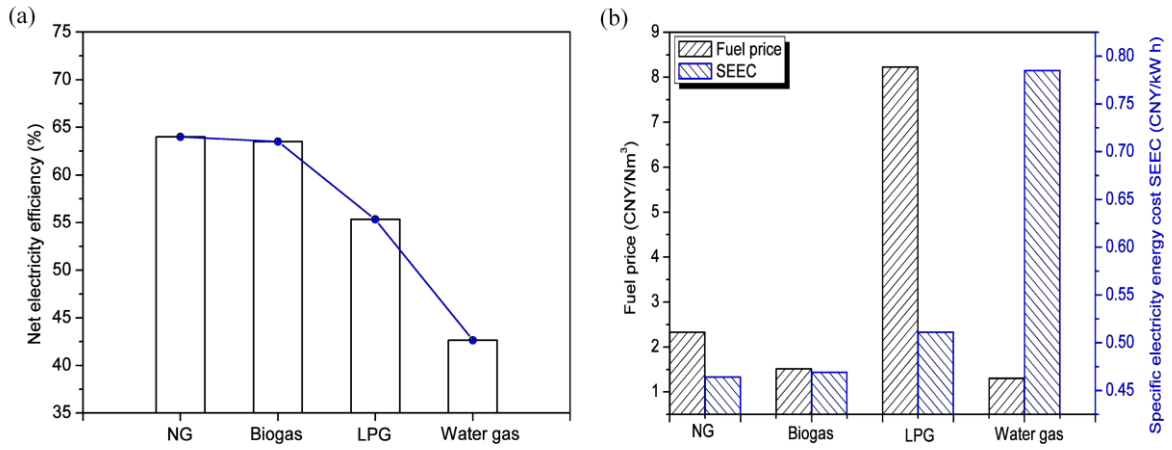

Fig. 11. Comparison of techno-economic performance between the SOFC-WGS-TSA-PEMFC hybrid system with different fuels. (a) The net electricity efficiency; (b) The fuel price and SEEC.

In fact, many countries encourage to develop NG and biogas fuels as clean energy resources. Various subsidy policies about the distributed power generation system using the NG or biogas fuels have been carried out in different countries. Taking Shanghai city of Eastern China (illustrated in Fig. 12) as an example, this city encourages the development of the medium- and large-scale distributed electricity power generation system using NG and biogas as the fuel. Chinese central government issued the subsidy policy of at least 10% of the electricity cost for the project with the power generation of less than 20 MWe and more than 20% subsidy for the power in the range of 20~50 MWe in 2017 (China, 2017). Besides the central government policy, the regional government has also decided to raise the subsidy levels on the medium- and large-scale projects. For example, in Shanghai, the standard subsidy level is 2000 CNY/kW for the NG project with the operation time over of 2000 h/year and 2500 CNY/kW when the operation time is over 3000 h/year (Government, 2017). The upper limit for the subsidy on each NG project is up to 50 million CNY. In this paper, the operation time of the NG-fed SOFC-WGS-TSA-PEMFC hybrid system is 8760 h, which is much more than

3000 h/year. The amount of power generation is 10 MWe. Accordingly, the regional subsidy level is calculated to be 25 million CNY for the NG-fed hybrid system proposed in this work, which is also lower than the upper limit of the subsidy on each project. On the other hand, the eastern China regional government also raised the subsidy policy to support the biogas project, which is 1500 CNY/Nm^3 as the subsidy for the power plants with the biogas production of at least 500 Nm^3/day and 2500 CNY/Nm^3 for the plants with daily yields of 10000 Nm^3 biogas (Chen and Liu, 2017; China, 2015). The upper limit for the subsidy on each biogas project is also 50 million CNY. In this work, the daily yields of biogas is calculated to be over 58000 Nm^3. Therefore, the subsidy level of the biogas-fed hybrid system is the upper limit of the subsidy of each project, which is 50 million CNY.

Fig. 12. General location of Eastern China and the exact location of Shanghai city in our case

Taking these financial subsidies into account, the SEEC of the SOFC-WGS-TSA-PEMFC hybrid system fed by the NG or biogas can be further reduced. Under the current central government subsidy, the SEEC of the hybrid system is reduced to 0.418 and 0.422 CNY/kW h for the NG and biogas projects, respectively. Furthermore, the combination of central and regional subsidy reduces the SEEC of the NG- and biogas-fed hybrid systems by 16% and 22% , respectively. Accordingly, the payback period is shortened from 2.6 to 1.5 year (NG) and from 2.5 to 0.8 year (biogas), as illustrated in Fig. 13. The annual return on investment

(ROI) is increased from 6.49% to 9.67% (NG) and from 6.33% to 10.98% (biogas) caused by the stimulation of the central and regional subsidy. Herein, the central subsidy contributes to the payback period of 2.1 year and the annual ROI of 8.33% for the NG project as well as 2.0 year and 8.14% for the biogas project. For comparison, the payback period and the annual ROI of the 10 MWe LPG-fed SOFC-WGS-TSA-PEMFC hybrid system are calculated to be 2.9 year and 4.98%, which presents the worse investment economy compared to the NG and biogas projects. For the water gas project, the SEEC value (0.785 CNY/kW h) is a little higher than the present market electricity cost 0.7655 CNY/kW h in Shanghai, indicating that the water gas project for distributed power plant is not economically competitive in Shanghai. Therefore, the results of payback period and annual ROI further confirm that the NG and biogas are the cost-optimal fuels for the SOFC-WGS-TSA-PEMFC hybrid power generation system.

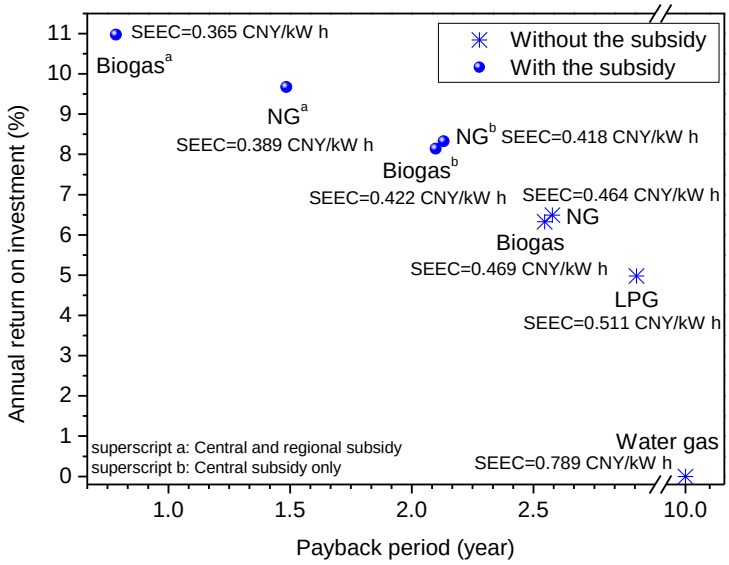

Fig. 13. The annual return on investment and payback period of the different SOFC-WGS-TSA-PEMFC hybrid electricity power generation systems with/without subsidy.

It can be also seen in Fig. 13 that the NG project has the comparable investment economy to the biogas project without the subsidy or with the central subsidy. However, these two projects present a large difference in the payback period and annual ROI when the regional subsidy is included. This is mainly because of the different regional subsidy policies on the NG and biogas projects. In this paper, the regional subsidy of the 10 MWe biogas-fed SOFC-WGS-

TSA-PEMFC hybrid system is more than twice of that by the NG-fed system at the same power level. Therefore, depending on the power scale, the subsidy level has a significant impact on the investment economy of the SOFC-WGS-TSA-PEMFC hybrid system. Fig. 14 displays the techno-economic performance of the NG- and biogas-fed hybrid systems with different scales under the subsidy. The biogas-fed hybrid system has the lower SEEC than the NG-fed hybrid system at the power scale of 10 MWe, while the SEEC of the NG power generation system becomes slightly smaller with the power scale more than 20 MWe. Accordingly, the biogas power generation system with 10 MWe power has the shorter payback period and the higher annual ROI than the NG project with the same small power level. However, the NG system has a slightly shorter payback period and a higher annual ROI for large scale power generation (more than 30 MWe). The variation tendency of techno-economic performance with the increase of power scale shown in Fig. 14 b, is mainly ascribed to different subsidy policies on the NG and biogas power generation projects. When the power scale is 10 MWe, the central subsidy for the NG or biogas project allows for a 10% discount on the specific electricity cost. When the power scale is over 20 MWe, the central subsidy level can be raised to a 20% discount. For the regional subsidy (Shanghai), the subsidy level is generally the upper limit (50 million CNY) for both NG and biogas projects over 20 MWe. In other words, the government encourage the development of the alternative fuels power generation project of 10~30 MWe power scale in the current situation. In the medium scale region Ⅱ, these two fuel power generation systems have comparable techno-economic performance. Take the power scale of 20 MWe as an example, the SEEC of the NG project is found to be 0.384 CNY/kW h, while the SEEC value of the biogas counterpart is 0.390 CNY/kW h, as shown in Fig. 14 a. Accordingly, the 20 MWe NG project has the payback period of 1.37 year and the annual ROI of 9.93%. By comparison, the payback period and annual ROI of the biogas project are 1.36 year and 9.64%. The comparable techno-economic performance between the NG and biogas power generation projects is mainly because of the same subsidy level for the NG and biogas projects, both of which reach the upper limit (50 million CNY) in the medium scale region. At the larger power scale, the subsidy remains unchanged, so the average power subsidy inevitably reduces with the increase of the power. Thus, the economy of the NG and biogas power

generation system becomes worse in the large-scale region Ⅲ. Therefore, the technology roadmap of the NG- and biogas-fed SOFC-WGS-TSA-PEMFC hybrid system for distributed power generation in Eastern China can be summarized according to the current subsidy as below:

1. For small scale power generation project, it is cost-optimal to develop the biogas-fed hybrid system. The specific electricity cost (0.365 CNY/kW h) is lower than the present feed-in tariff (FIT) price (0.475~0.704 CNY/kW h) for biogas power generation in China and the FIT price (~0.65 CNY/kW h) in Shanghai.
2. In the medium scale region, the NG power generation project has the comparable techno-economic performance to the biogas project.
3. For the large scale power generation, the NG-fed SOFC-WGS-TSA-PEMFC hybrid system is preferentially considered in eastern China. The specific electricity cost also remains stable, which is 0.345~0.347 CNY/kW h much smaller than the on-grid electricity cost 0.7655 CNY/kW h in Shanghai.

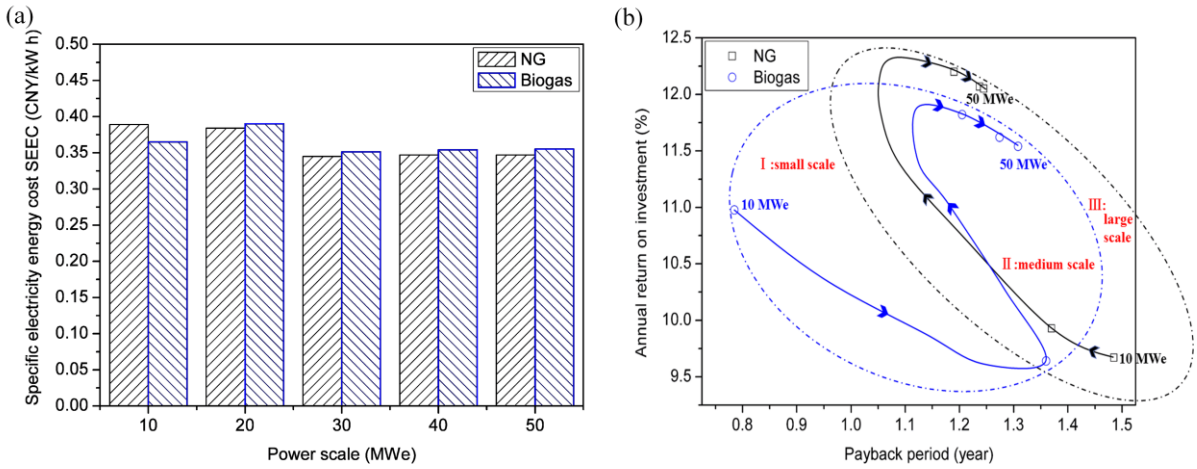

Fig. 14. The techno-economic performance of the NG- and biogas-fed SOFC-WGS-TSA-PEMFC hybrid systems with different scales under the subsidy. (a) The SEEC; (b) The annual return on investment and payback period.

5. Conclusions

In summary, this work proposes a novel SOFC-WGS-TSA-PEMFC hybrid system for power generation and evaluates its economic feasibility under different fuel options. Furthermore, the development roadmap of this kind of power generation technology is proposed using Eastern China as a case study. The following conclusions can be drawn:

1) The system using NG or biogas as fuel has a high efficiency up to 63.5~64%, while using LPG or water gas results in much lower efficiency. Accordingly, the electricity cost produced by this hybrid system can be lowered to 0.464~0.469 CNY/kW h.

2) The biogas-fed system is much more cost-optimal as a small-scale power generation device. For example, when considering energy consumers in Shanghai, the specific electricity cost is as low as 0.365 CNY/kW h, which is lower than present biogas power FIT price 0.475~0.704 CNY/kW h in China. The payback period and the annual return on investment are found to be 0.8 year and 11%, respectively.

3) The NG-fed system is more suitable for the large-scale power generation under the subsidy. The specific electricity cost is 0.345~0.347 CNY/kW h, which is much smaller than the on-grid electricity price in Shanghai (0.7655 CNY/kW h). The payback period and the annual return on investment are 1.2 year and 12%, respectively.

The proposed SOFC-PEMFC hybrid system is indeed efficient and economical for power generation as demonstrated in this paper. However, there are still some technical issues needed to address in the future, which are briefly summarized as follows: 1) The biogas purification is not considered in this study; 2) The dynamic behavior is unclear when this system is used as a distributed power plant for peak clipping and valley filling in the power demand profiles; 3) The development roadmap of the proposed hybrid power generation technology under different regions of China is unrevealed. Actually, the regional subsidy level for biogas or natural gas power project at different regions is discrepant, which generally depends on the regional economic level and the regional resources of biogas or natural gas. Therefore, the future directions can focus on the above-mentioned aspects for the proposed hybrid power system.

Acknowledgments

Z. Wu thanks the funding support from Hong Kong Scholar Program (XJ2017023) and the National Natural Science Foundation of China (21736008). P. Tan thanks the funding support from CAS Pioneer Hundred Talents Program and USTC Tang Scholar. M. Ni thanks the funding support (Project Number: PolyU 152214/17E) from Research Grant Council, University Grants Committee, Hong Kong SAR.

Appendix A

Table A1. The capital cost model of all the components of the SOFC-WGS-TSA-PEMFC hybrid electricity power generation system (Thomas, 1999; Arsalis, 2008; Chitsaz et al., 2015).

Capital cost	Description	Capital cost equations
C_{SOFC}	Cost of SOFC stack	$C_{SOFC} = C_{Stack} + C_{AUX} + C_{INV}$ $C_{Stack} = A_{cell} \cdot \left(2.96 \cdot T_{SOFC} - 1907\right)$ $C_{INV} = 10^5 \cdot \left(\frac{W_{SOFC}}{500}\right)^{0.70}$ $C_{AUX} = 0.1 \cdot C_{Stack}$
C_{PEM}	Cost of PEMFC stack	$C_{PEM} = C_{Stack} + C_{AUX} + C_{INV}$ $C_{Stack} = b_1 \cdot \left[\left(\frac{b_2 - 105.4}{10} + 1437.3 \cdot L_{Pt} \cdot C_{Pt}\right) \cdot \frac{A_{cell} \cdot (1+\theta)^{\lambda}}{1000} + b_3\right]$ $C_{INV} = 10^5 \cdot \left(\frac{W_{PEM}}{500}\right)^{0.70}$ $C_{AUX} = c_1 + c_2 \cdot W_{PEM} - c_3 \cdot {W_{PEM}}^2$
C_{WGS}	Cost of WGS reactors	$C_{WGS} = C_{WGS-reac} + C_{WGS-cata}$

		$C_{WGS-reac} = C_{ref} \cdot \beta \cdot \left(\frac{U_{WGS}}{U_{ref}} \right)^{\gamma}$
		$C_{WGS-cata} = U_{Cata} \cdot C_{Cata}$
		$\beta = a_1 + a_2 \cdot \beta_m \cdot \beta_p$
		$\beta_p = d_0 + d_1 \cdot \log(p) + d_2 \cdot \log(p)^2 + d_3 \cdot \log(p)^6 + d_4 \cdot \log(p)^8$
		$U_{WGS} = U_{factor} \cdot U_{Cata}$
		$U_{Cata} = \frac{\phi_{in}}{\rho_{Cata}} \int_{X=0}^{X=X_r} \frac{dX}{-r}$
		$r = -k \cdot \exp(-\frac{E_{act}}{RT}) \cdot (p_{CO})^{\alpha_{CO}} \cdot (p_{H_2O})^{\alpha_{H_2O}}$
C_{comp}	Cost of compressor	$C_{comp} = 91562 \left(\dot{W}_{comp} / 445 \right)^{0.67}$
C_{HE}	Cost of heat exchanger	$C_{HE} = 130 \cdot \left(\frac{A_{HE}}{0.093} \right)^{0.78}$
		$C_{TSA} = C_{MH} + C_{reac}$
C_{TSA}	Cost of TSA reactor	$C_{MH} = \frac{3600 \cdot \phi_{H_2} \cdot t_{oper}}{\psi_{MH} \cdot n_{cycle} \cdot t_{cycle}} \cdot \omega_{MH}$
		$C_{reac} = U_{316L} \cdot \rho_{316L} \cdot C_{316L}$

Table A2. The values of the important parameters shown in the capital cost equations of all the components. (Levenspiel, 1972; Turton, 1998; Marechal et al., 2005)

Parameter	Description	Value
b_1		1.1
b_2	Constants for PEMFC stack cost calculation	811.77
b_3		1311.3
c_1	Constants for PEMFC auxiliary components cost	3343.5 $
c_2	calculation	39.942 $/kW

c_3			0.0454 \$/kW^2
θ	FC degradation factor		6% /year
λ	Cycle life		10 years
L_{Pt}	The amount of catalyst Pt load		0.6 mg/cm^2
C_{Pt}	Catalyst Pt cost		0.0122 \$/mg
a_1	Coefficients for calculating the scale proportionality factor		1.62
a_2			1.47
d_0	Coefficients for calculating the pressure factor		0.5146
d_1			0.6838
d_2			0.297
d_3			0.0235
d_4			0.002
β_m	Material factor		1
U_{ref}	Volume of the reference case reactor		0.104 m^3
C_{ref}	Cost of the reference case reactor		5774 \$
U_{factor}	Volume factor		1.17
γ	Scale exponent		0.59
k	HT-WGS with the iron alumina catalyst	Frequency factor of catalyst	108 kmol/kg/s/bar
E_{act}		Activation energy of catalyst	80.386 kJ/mol
C_{Cata}		Cost of catalyst	100000 \$/m^3
ρ_{Cata}		Bulk density of catalyst	1200 kg/m^3
α_{CO}		Partial pressure order for reactant CO	0.58
α_{H_2O}		Partial pressure order for reactant H_2O	0.04
k	LT-WGS with the nickel alumina catalyst	Frequency factor of catalyst	390 kmol/kg/s/bar
E_{act}		Activation energy of catalyst	78.293 kJ/mol
C_{Cata}		Cost of catalyst	100000 \$/m^3

ρ_{Cata}	Bulk density of catalyst	1200 kg/m^3
α_{CO}	Partial pressure order for reactant CO	-0.14
α_{H_2O}	Partial pressure order for reactant H_2O	0.62

Table A3. The annual cost models used in the thermo-economic modeling of the SOFC-WGS-TSA-PEMFC hybrid system. (Arsalis, 2008; Peters and Timmerhaus, 2003)

Annual cost composition	Model equation	Parameter
Depreciation cost C_{Depr}	$C_{Depr} = \frac{C_{Capt}}{\lambda}$	λ : cycle life, 10 years
Operation cost C_{Oper}	$C_{Oper} = \phi_{NG} \cdot \pi_{NG} \cdot \frac{t_{oper}}{\lambda}$	ϕ_{NG} : Flue flux, Nm^3/h π_{NG} : Fuel price, CNY/Nm^3 t_{oper} : Total operating time, 8760 h
Maintenance cost C_{Main}	$C_{Main} = \frac{C_{Capt}}{\lambda} \cdot f_{Main}$	f_{Main} : Maintenance factor, 0.06
Investment interest cost C_{Int}	$C_{Int} = \frac{C_{Capt}}{\lambda} \cdot f_{Int}$	f_{Int} : Interest factor, 0.0926
Insurance cost C_{Ins}	$C_{Ins} = \frac{C_{Capt}}{\lambda} \cdot f_{Ins}$	f_{Ins} : Insurance factor, 0.20
Tax cost C_{Tax}	$C_{Tax} = \frac{C_{Capt}}{\lambda} \cdot f_{Tax}$	f_{Tax} : Tax factor, 0.05
Total annual cost C_{TOTAL}	$C_{TOTAL} = C_{Depr} + C_{Oper} + C_{Main} + C_{Int} + C_{Ins} + C_{Tax}$	

References

Aguiar, P., Adjiman, C.S., Brandon, N.P., 2004. Anode-supported intermediate temperature direct internal reforming solid oxide fuel cell. I: model-based steady-state performance. J. Power Sources. 138, 120–136. https://doi.org/10.1016/j.jpowsour.2004.06.040

Ahn, S., You, Y.W., Lee, D.G., Kim, K.H., Oh, M., Lee, C.H., 2012. Layered two- and four-bed PSA processes for H_2 recovery from coal gas. Chem. Eng. Sci. 68, 413–423. https://doi.org/10.1016/j.ces.2011.09.053

Arsalis, A., 2008. Thermoeconomic modeling and parametric study of hybrid SOFC–gas turbine–steam turbine power plants ranging from 1.5 to 10 MWe. J. Power Sources 181, 313–326. https://doi.org/10.1016/j.jpowsour.2007.11.104

Barutha, P., Nahvi, A., Cai, B., Jeong, H.D., Sritharan, S., 2019. Evaluating commercial feasibility of a new tall wind tower design concept using a stochastic levelized cost of energy model. J. Clean. Prod. 240. https://doi.org/10.1016/j.jclepro.2019.118001

Bellosta von Colbe, J.M., Puszkiel, J., Capurso, G., Franz, A., Benz, H.U., Zoz, H., Klassen, T., Dornheim, M., 2019. Scale-up of milling in a 100 L device for processing of TiFeMn alloy for hydrogen storage applications: Procedure and characterization. Int. J. Hydrogen Energy. https://doi.org/10.1016/j.ijhydene.2019.01.174

Calbry-Muzyka, A.S., Gantenbein, A., Schneebeli, J., Frei, A., Knorpp, A.J., Schildhauer, T.J., Biollaz, S.M.A., 2019. Deep removal of sulfur and trace organic compounds from biogas to protect a catalytic methanation reactor. Chem. Eng. J. 360, 577–590. https://doi.org/10.1016/j.cej.2018.12.012

Chan, S.H., Ho, H.K., Tian, Y., 2002. Modelling of simple hybrid solid oxide fuel cell and gas turbine power plant. J. Power Sources 109, 111–120. https://doi.org/10.1016/S0378-7753(02)00051-4

Cheddie, D.F., 2010. Integration of a solid oxide fuel cell into a 10 MW gas turbine power plant. Energies 3, 754–769. https://doi.org/10.3390/en3040754

Chen, Q., Liu, T., 2017. Biogas system in rural China: Upgrading from decentralized to centralized? Renew. Sustain. Energy Rev. 78, 933–944. https://doi.org/10.1016/j.rser.2017.04.113

China, M. of A.D. and R.C. of, 2015. Work Plan Transform Upgrade Rural Biogas Project. URL http://www.ndrc.gov.cn/fzgggz/ncjj/zhdt/201504/t20150423_689025.html (accessed 4.23.15).

China, N.D. and R.C. and N.E.A. of, 2017. Pilot Projects for Market-Oriented Reforms for Distributed Power Generation. URL http://zfxxgk.nea.gov.cn/auto87/201711/W020171113589438141944.docx (accessed 10.31.17).

China, N.D. and R.C. and N.E.A. of, 2016. Thirteen Five-Year Plan on Natural Gas Development. URL http://www.ndrc.gov.cn/zcfb/zcfbtz/201701/W020170119333355283662.pdf (accessed 12.24.16).

Chitsaz, A., Mehr, A.S., Mahmoudi, S.M.S., 2015. Exergoeconomic analysis of a trigeneration system driven by a solid oxide fuel cell. Energy Convers. Manag. 106, 921–931. https://doi.org/10.1016/j.enconman.2015.10.009

Congress US, 2005. Energy policy act of 2005. Public Law 109-58. URL https://www.congress.gov/109/plaws/publ58/PLAW-109publ58.pdf (accessed 8.8.05).

Correa, J.M., Farret, F.A., Canha, L.N., Simoes, M.G., 2004. An electrochemical-based fuel-cell model suitable for electrical engineering automation approach. IEEE Trans. Ind. Electron. 51, 1103–1112. https://doi.org/10.1109/TIE.2004.834972

Cruz, M.A., Araujo, O.Q.F., de Medeiros, J.L., de Paula, R., de Castro, V., Ribeiro, G.T., de Oliveira, V.R., 2017. Impact of solid waste treatment from spray dryer absorber on the levelized cost of energy of a coal-fired power plant. J. Clean. Prod. 164, 1623–1634. https://doi.org/10.1016/j.jclepro.2017.07.061

Cui, X., Kær, S.K., 2018. Thermodynamic analysis of steam reforming and oxidative steam reforming of propane and butane for hydrogen production. Int. J. Hydrogen Energy 43, 13009–13021. https://doi.org/10.1016/j.ijhydene.2018.05.083

Damo, U.M., Ferrari, M.L., Turan, A., Massardo, A.F., 2019. Solid oxide fuel cell hybrid system: A detailed review of an environmentally clean and efficient source of energy. Energy 168, 235–246. https://doi.org/10.1016/j.energy.2018.11.091

Ferguson, J.R., Fiard, J.M., Herbin, R., 1996. Three-dimensional numerical simulation for various geometries of solid oxide fuel cells. J. Power Sources 58, 109–122. https://doi.org/10.1016/0378-7753(95)02269-4

Fernandes, A., Woudstra, T., van Wijk, A., Verhoef, L., Aravind, P.V., 2016. Fuel cell electric vehicle as a power plant and SOFC as a natural gas reformer: An exergy analysis of different system designs. Appl. Energy 173, 13–28. https://doi.org/10.1016/j.apenergy.2016.03.107

Feron, P., Cousins, A., Jiang, K., Zhai, R., Shwe Hla, S., Thiruvenkatachari, R., Burnard, K., 2019. Towards Zero Emissions from Fossil Fuel Power Stations. Int. J. Greenh. Gas Control 87, 188–202. https://doi.org/10.1016/j.ijggc.2019.05.018

Fiorentino, G., Zucaro, A., Ulgiati, S., 2019. Towards an energy efficient chemistry. Switching from fossil to bio-based products in a life cycle perspective. Energy 170, 720–729. https://doi.org/10.1016/j.energy.2018.12.206

Fiori, C., Dell'Era, A., Zuccari, F., Santiangeli, A., D'Orazio, A., Orecchini, F., 2015. Hydrides for submarine applications: Overview and identification of optimal alloys for air independent propulsion maximization. Int. J. Hydrogen Energy 40, 11879–11889. https://doi.org/10.1016/j.ijhydene.2015.02.105

Gholamian, E., Habibollahzade, A., Zare, V., 2018. Development and multi-objective optimization of geothermal-based organic Rankine cycle integrated with thermoelectric generator and proton exchange membrane electrolyzer for power and hydrogen production. Energy Convers. Manag. 174, 112–125. https://doi.org/10.1016/j.enconman.2018.08.027

Golmakani, A., Fatemi, S., Tamnanloo, J., 2017. Investigating PSA, VSA, and TSA methods in SMR unit of refineries for hydrogen production with fuel cell specification. Sep. Purif. Technol. 176, 73–91. https://doi.org/10.1016/j.seppur.2016.11.030

Government, S.M.P., 2017. Procedures of Shanghai Municipality Regarding Special Subsidies to Promote Natural Gas Distributed Energy Supply Systems and Gas Air-conditioners. URL http://www.shanghai.gov.cn/nw2/nw2314/nw2319/nw12344/u26aw50959.html (accessed 1.3.17).

Habibollahzade, A., Gholamian, E., Houshfar, E., Behzadi, A., 2018. Multi-objective optimization of biomass-baded solid oxide fuel cell integrated with Stirling engine and electrolyzer. Energy Convers. Manag. 171, 1116–1133. https://doi.org/10.1016/j.enconman.2018.06.061

Habibollahzade, A., Gholamian, E., Behzadi, A., 2019. Multi-objective optimization and comparative performance analysis of hybrid biomass-based solid oxide fuel cell/solid oxide electrolyzer cell/gas turbine using different gasification agents. Appl. Energy 233-234, 985–1002. https://doi.org/10.1016/j.apenergy.2018.10.075

International Energy Agency, 2018. 2018 World Energy Outlook: Executive Summary. Oecd/Iea 11.

Jemni, A., 1999. Experimental and theoretical study of ametal–hydrogen reactor. Int. J. Hydrogen Energy 24, 631–644. https://doi.org/10.1016/S0360-3199(98)00117-7

Kuckshinrichs, W., Koj, J.C., 2018. Levelized cost of energy from private and social perspectives: The case of improved alkaline water electrolysis. J. Clean. Prod. 203, 619–632. https://doi.org/10.1016/j.jclepro.2018.08.232

Levenspiel, O., 1972. Chemical Reaction Engineering. John Wiley and Sons, New York.

Liu, Y., Han, J.T., You, H.L., 2018. Performance analysis of a CCHP system based on SOFC/GT/CO_2 cycle and ORC with LNG cold energy uitlization. Int. J. Hydrogen Energy 44, 29700–29710. https://doi.org/10.1016/j.ijhydene.2019.02.201

Lv, X.J., Ding, X.Y., Weng, Y.W., 2019. Effect of fuel composition fluctuation on the safety performance of an IT-SOFC/GT hybrid system. Energy 174, 45–53. https://doi.org/10.1016/j.energy.2019.02.083

Marechal, F., Palazzi, F., Godat, J., Favrat, D., 2005. Thermo-economic modelling and optimisation of fuel cell systems. Fuel Cells 5, 5–24. https://doi.org/10.1002/fuce.200400055

Massardo, A.F., Lubelli, F., 2000. Internal Reforming Solid Oxide Fuel Cell-Gas Turbine Combined Cycles (IRSOFC-GT): Part A—Cell Model and Cycle Thermodynamic Analysis. J. Eng. Gas Turbines Power 122, 27–35. https://doi.org/10.1115/1.483187

Mehrpooya, M., Sayyad, S., Zonouz, M.J., 2017a. Energy, exergy and sensitivity analyses of a hybrid combined cooling, heating and power (CCHP) plant with molten carbonate fuel cell (MCFC) and Stirling engine. J. Clean. Prod. 148, 283–294. https://doi.org/10.1016/j.jclepro.2017.01.157

Mehrpooya, M., Ansarinasab, H., Sharifzadeh, M.M.M., Rosen, M.A., 2017b. Process development and exergy cost sensitivity analysis of a hybrid molten carbonate fuel cell power plant and carbon dioxide capturing process. J. Power Sources. 364, 299–315. https://doi.org/10.1016/j.jpowsour.2017.08.024

Mehrpooya, M., Ansarinasab, H., Sharifzadeh, M.M.M., Rosen, M.A., 2018a. Conventional and advanced exergoeconomic assessments of a new air separation unit integrated with a carbon dioxide electrical power cycle and a liquefied natural gas regasification unit. Energy Convers. Manag. 163, 151–168. https://doi.org/10.1016/j.enconman.2018.02.016

Mehrpooya, M., Sharifzadeh, M.M.M., Zonouz, M.J., Rosen, M.A., 2018b. Cost and economic potential analysis of a cascading power cycle with liquefied natural gas regasification. Energy Convers. Manag. 156, 68–83. https://doi.org/10.1016/j.enconman.2017.10.100

Meng, Y., Jiang, J., Gao, Y., Aihemaiti, A., Ju, T., Xu, Y., Liu, N., 2019. Biogas upgrading to methane: Application of a regenerable polyethyleneimine-impregnated polymeric resin (NKA-9) via CO_2 sorption. Chem. Eng. J. 361, 294–303. https://doi.org/https://doi.org/10.1016/j.cej.2018.12.091

Muthukumar, P., Prakashmaiya, M., Murthy, S., 2005. Experiments on a metal hydride-based hydrogen storage device. Int. J. Hydrogen Energy 30, 1569–1581. https://doi.org/10.1016/j.ijhydene.2004.12.007

Ni, M., Leung, M.K.H., Leung, D.Y.C., 2007. Parametric study of solid oxide fuel cell performance. Energy Convers. Manag. 48, 1525–1535. https://doi.org/10.1016/j.enconman.2006.11.016

Owebor, K., Oko, C.O.C., Diemuodeke, E.O., Ogorure, O.J., 2019. Thermo-environmental and economic analysis of an integrated municipal waste-to-energy solid oxide fuel cell, gas-, steam-, organic fluid- and absorption refrigeration cycle thermal power plants. Appl. Energy 239, 1385–1401. https://doi.org/10.1016/j.apenergy.2019.02.032

Panwar, K., Srivastava, S., 2018. Investigations on calculation of heat of formation for multi-element AB_5 -type hydrogen storage alloy. Int. J. Hydrogen Energy 43, 11079–11084. https://doi.org/10.1016/j.ijhydene.2018.04.213

Peters, M.S., Timmerhaus, K.D., 2003. Plant Design and Economics for Chemical Engineers. McGraw-Hill, New York.

Rabbani, A., Rokni, M., 2014. Modeling and analysis of transport processes and efficiency of combined SOFC and PEMFC systems. Energies 7, 5502–5522. https://doi.org/10.3390/en7095502

Reiser, A., 2000. The application of Mg-based metal-hydrides as heat energy storage systems. Int. J. Hydrogen Energy 25, 425–430. https://doi.org/10.1016/S0360-3199(99)00057-9

Rossi, I., Traverso, A., Tucker, D., 2019. SOFC/Gas turbine hybrid system: A simplified framework for dynamic simulation. Appl. Energy 238, 1543–1550. https://doi.org/10.1016/j.apenergy.2019.01.092

Samanta, S., Ghosh, S., 2017. Techno-economic assessment of a repowering scheme for a coal fired power plant through upstream integration of SOFC and downstream integration of MCFC. Int. J. Greenhouse Gas Control 64, 234–245. https://doi.org/10.1016/j.ijggc.2017.07.020

Sedghisigarchi, K., Feliachi, A., 2004. Dynamic and transient analysis of power distribution systems with fuel cells—Part I: Fuel-cell dynamic model. IEEE T. Energy Conver. 19, 423–428. https://doi.org/10.1109/TEC.2004.827039

Sghaier, S.F., Khir, T., Brahim, A.B., 2018. Energetic and exergetic parametric study of a SOFC-GT hybrid power plant. Int. J. Hydrogen Energy 43, 3542–3554. https://doi.org/10.1016/j.ijhydene.2017.08.216

SparX, D.A.I., 2018. China gas utilities sector. URL https://www.dbs.com/aics/pdfController.page?pdfpath=/content/article/pdf/AIO/072018/180727_insights_integrated_energy_market_vast_potential_for_gas_distributors.pdf (accessed 7.27.18).

Srivastava, S., Upadhyaya, R.K., 2011. Investigations of AB_5-type hydrogen storage materials with enhanced hydrogen storage capacity. Int. J. Hydrogen Energy 36, 7114–7121. https://doi.org/10.1016/j.ijhydene.2011.02.111

Stiller, C., Thorud, B., Seljebø, S., Mathisen, Ø., Karoliussen, H., Bolland, O., 2005. Finite-volume modeling and hybrid-cycle performance of planar and tubular solid oxide fuel cells. J. Power Sources 141, 227–240. https://doi.org/10.1016/j.jpowsour.2004.09.019

Tang, S., Amiri, A., Vijay, P., Tadé, M.O., 2016. Development and validation of a computationally efficient pseudo 3D model for planar SOFC integrated with a heating furnace. Chem. Eng. J. 290, 252–262. https://doi.org/10.1016/j.cej.2016.01.040

Tarasov, B.P., Bocharnikov, M.S., Yanenko, Y.B., Fursikov, P.V., Lototskyy, M.V., 2018. Cycling stability of RNi_5 (R = La, La+Ce) hydrides during the operation of metal hydride hydrogen compressor. Int. J. Hydrogen Energy 43, 4415–4427. https://doi.org/10.1016/j.ijhydene.2018.01.086

The World Bank, 2018. Global Development Data. URL https://data.worldbank.org/

Thomas, C.E., 1999. Cost analysis of stationary fuel cell systems including hydrogen co-generation. Dir. Technol. URL https://www.directedtechnologies.com

Turton, R., 1998. Analysis, Synthesis and Design of Chemical Processes. Prentice Hall, NJ.

U.S. DOE, 2015. Multi-year research, development, and demonstration plan – Part 3.3 hydrogen storage. Fuel Cell Technologies Office. URL https://www.energy.gov/sites/prod/files/2015/05/f22/fcto_myrdd_storage.pdf

U.S. Energy Information Administration, 2019. Daily prices. URL https://www.eia.gov/todayinenergy/prices.php (accessed 8.2.19).

Vazquez, A., Iglesias, G., 2015. LCOE (levelised cost of energy) mapping: A new geospatial tool for tidal stream energy. Energy 91, 192–201. https://doi.org/10.1016/j.energy.2015.08.012

Vollmar, H.E., Maier, C.U., Nölscher, C., Merklein, T., Poppinger, M., 2008. Innovative concepts for the coproduction of electricity and syngas with solid oxide fuel cells. J. Power Sources. 86, 90–97. https://doi.org/10.1016/S0378-7753(99)00421-8

Wang, Q., Su, M., Li, R., Ponce, P., 2019. The effects of energy prices, urbanization and economic growth on energy consumption per capita in 186 countries. J. Clean. Prod. 225, 1017–1032. https://doi.org/10.1016/j.jclepro.2019.04.008

Wu, Z., Zhang, Z., Ni, M., 2018. Modeling of a novel SOFC-PEMFC hybrid system coupled with thermal swing adsorption for H_2 purification: Parametric and exergy analyses. Energy Convers. Manag. 174, 802–813. https://doi.org/10.1016/j.enconman.2018.08.073

Wu, Z., Tan, P., Chen, B., Cai, W., Chen, M., Xu, X., Zhang, Z., Ni, M., 2019a. Dynamic modeling and operation strategy of an NG-fueled SOFC-WGS-TSA-PEMFC hybrid energy conversion system for fuel cell vehicle by using MATLAB/SIMULINK. Energy 175, 567–579. https://doi.org/10.1016/j.energy.2019.03.119

Wu, Z., Zhu, P.F., Yao, J., Tan, P., Xu, H.R., Chen, B., Yang, F.S., Zhang, Z.X., Ni, M., 2019b. Thermo-economic modeling and analysis of an NG-fueled SOFC-WGS-TSA-PEMFC hybrid energy conversion system for stationary electricity power generation. Energy, https://doi.org/10.1016/j.energy.2019.116613

Xiong, F.L., Zhu, H.G., Shi, H.R., Wu, J., 2011. Analysis on the price of the biogas for rural centralized biogas plan. China Biogas 29, 16–19.